Perspective

Multipartite continuous-variable optical quantum entanglement: Generation and application

Warit Asavanant [*] and Akira Furusawa [†]

Department of Applied Physics, School of Engineering, The University of Tokyo, 7-3-1 Hongo, Bunkyo-ku, Tokyo 113-8656, Japan and Optical Quantum Computing Research Team, RIKEN Center for Quantum Computing, 2-1 Hirosawa, Wako, Saitama 351-0198, Japan

(Received 13 June 2023; published 9 April 2024)

Quantum entanglement is a fundamental resource for various quantum applications and generation of large-scale entanglement is a key quantum technology. In recent years, continuous-variable optical systems have shown promising results in this direction, thanks to deterministic generation and multiplexing via rich degrees of freedom naturally occurring in the optical system. In this paper, we review the generation and applications of multipartite optical quantum entanglement. We begin with a theoretical overview of how to represent and verify multimode continuous-variable quantum states and entanglement. Then, we discuss the multiplexing technique in time, frequency, and spatial domains, and their applications in generation of large-scale entangled states. Afterward, we review the current status and development of the basic technology used in the generation of multipartite quantum entanglement. Finally, we discuss the applications of large-scale quantum entanglement and possible future perspectives.

DOI: 10.1103/PhysRevA.109.040101

I. INTRODUCTION

Quantum physics plays an important role in the development of science and technology. In quantum mechanics, many ideas foreign to classical physics are introduced to explained physical phenomena on the microscopic level. These ideas, although counterintuitive, have withstood countless experiments and are incorporated in a current standard framework of physics. Quantum mechanics are now used not only to describe physical phenomena, but to control and engineer the physical systems for various novel applications such as quantum computation [1,2], quantum communication [3,4], quantum cryptography [5], quantum chemistry [6], quantum material [7], to name a few.

One of the ideas central to quantum mechanics is quantum entanglement. The concept of quantum entanglement arises when two or more quantum systems are considered. When multiple quantum systems interact with each other, the resultant quantum state can become inseparable, even after each system is physically separated. The observable effects of the inseparability of the quantum state appear when each system is measured and the correlation between the measurement results is investigated; due to the property of quantum entanglement, the measurement results are likely correlated. In fact, they can be correlated in a way that cannot be explained within the standard framework of classical mechanics. An important example of this is the violation of Bell inequality, an inequality that holds in the classical regime, with quantum entanglement [8,9]. Although we will properly define quantum entanglement later, we would like to note to the reader that there are concepts such as steering [10] and nonlocality [11] that are closely related to quantum entanglement, but with different operational definition. In this article, our main focuses will be on practical generation and applications of quantum entanglement on optical systems and we will not delve into the details in the fundamentals of quantum mechanics.

The reason that makes quantum entanglement an intriguing concept is the fact that the observables of the quantum system can be locally random, but show more information (correlation) when they are considered as a whole. This correlation could even exist for physical quantities that are not locally commuted, meaning that the correlations can exist for not only a single observable but various observables that do not have local simultaneous eigenstate. In the paper by Einstein, Podolsky, and Rosen (EPR) in 1935, they argued that the prediction of the quantum entanglement itself is the internal contradiction of the quantum theory and the theory itself is incomplete [12]. Although the basic concepts of quantum mechanics are now widely accepted and the arguments by Einstein *et al.* are no longer a common view, a quantum state that appeared in their argument, the EPR state, has now become one of the most important quantum entangled states. The coexistence of the local uncertainty principle and the multipartite quantum entanglement is the key to many of the quantum protocols such as quantum teleportation and quantum computation.

The experimental exploration of the quantum entanglement and its applications was accelerated by the pioneering work of Aspect, Clauser, and Zeilinger which was recognized in the Nobel prize in 2022. In addition to experimental detection of Bell pairs [13], the work by Zeilinger going beyond two-mode entanglement [14] and demonstration of quantum

[*] warit@alice.t.u-tokyo.ac.jp
[†] akiraf@ap.t.u-tokyo.ac.jp

teleportation with photonic entanglement [15] push the boundary of experimental development in quantum entanglement. Compared to many quantum systems, the photonic system provides a source of pure and clean quantum entanglement that can be easily manipulated at room temperature and atmospheric pressure. Subsequently, there are numerous works expanding the numbers and the structure of the quantum entanglement in the photonic qubit system [16]. The photonic entanglement generated by Aspect *et al.* belongs to an approach called discrete-variable (DV) approach. In this approach, the physical quantities take discrete values. Polarization qubit (S-pol or P-pol), time-bin qubit (which-time-bin information), and dual-rail qubit (which-path information) are examples of photonic DV systems.

A complementary approach to the DV approach is the continuous-variable (CV) approach [17]. In this approach, the physical quantities of interest have continuous spectrum rather than taking discrete values. In optical systems, such continuous spectrum naturally arises when one quantizes electromagnetic wave; the two quadrature operators (usually denoted $\hat{x}$ and $\hat{p}$) satisfy the commutation relation $[\hat{x}, \hat{p}] = i\hbar$, similar to position and momentum operator. Experimental development of the CV quantum entanglement began with the realization of the squeezed-light generation [18–21], one of the most fundamental quantum states of light in the generation of the CV quantum entanglement. Two-mode CV entanglement was used in the quantum teleportation protocol [22] and, subsequently, various generations of small-scale CV quantum entanglement in optical system have been realized and demonstrated over the years [23–35].

Although quantum entanglement in both DV and CV optical systems has seen astounding progresses, the recent idea of multiplexing changes the landscape of CV optical quantum entanglement from small scale to large scale. There are two main reasons that large-scale entanglement generation with multiplexing is highly compatible to the CV optical system. The first reason is the rich degrees of freedom of the optical system. There are many parameters in the optical system that can be incorporated to quantum computation. The examples are spatial mode, wavelength, path, polarization, temporal wave packet, time bin, to mention a few. Generation with multiplexing based on these degrees of freedom (or mixture of them) opens a gate to the large-scale entanglement generation. The propagating wave aspect of the optical system is also a crucial factor. Instead of making a qubit one by one, in the optical system, we make a circuit that generates entangled state when the light passes through. If such a circuit can be made so that various modes and degrees of freedom can interact, a large-scale entanglement can be generated using a simple circuitry. The core idea of multiplexing is that the same physical circuit can be used over and over for multiple light modes. The number of the research in the CV entanglement generation using multiplexing has increased over the years in both theory [36–50] and experiment [51–74], with various techniques based on various degrees of freedom being explored.

The second reason is that the squeezed-light generation is deterministic. The rich degree of freedom of the optical system is applicable to both DV and CV systems. On the other hand, large-scale entanglement generation based on multiplexing is much more progressed in the CV systems. The difference stems from the fact that single-photon generation in the optical systems is usually probabilistic, at the very best heralded, while the generation of squeezed light is deterministic. The deterministic nature of the squeezed-light source generation makes generation of quantum entanglement in the CV system highly advantageous as CV quantum entangled states can be generated with only the squeezed light and linear optics [75]. On the other hand, generation of DV entangled state uses a single-photon state which reduces the overall success probability when the scale of the entanglement increases. Many experimental and theoretical progresses are being made [76–78] which could improve the situation of the DV entanglement in the future. A related issue in the large-scale generation of entanglement in DV system is the nondeterministic nature of the DV Bell measurement, although these can be dealt with as the erasure error and corrected, given that overall probability and efficiency of the system is above a certain threshold [78].

From these two aspects, CV optical systems become natural physical systems for the generation of large-scale quantum entanglement. There are various theoretical formulations and experimental demonstrations over the recent years with many diverse approaches such as time domain, frequency domain, and spatial-mode multiplexing. In this paper, we will review the generation and application of the optical quantum entanglement, in particular for the CV system with the focus on the generation of the large-scale quantum entanglement beyond that of the traditional small-scale entanglement generation. The departure from small-scale entanglement to large-scale entanglement is an important step toward development of practical quantum technology.

This paper is structured as follows. We first give a general definition of quantum entanglement in Sec. II, then proceed to defining notation in the CV systems in Sec. III. After that, we define the multimode Gaussian state in Sec. IV and entanglement in Sec. V, and discuss how to evaluate and verify CV quantum entanglement. Section VI is the main topic of this paper, discussing how to generate large-scale quantum entanglement using various multiplexing techniques. The recent developments of the related components and experimental techniques are reviewed in Sec. VII. The applications of large-scale quantum entanglement and its future perspectives are discussed in Secs. VIII and IX, respectively.

II. DEFINITION

Formally, quantum entanglement is defined via the inseparability of the quantum state. If we consider two subsystem labels by A and B, these two systems are separable if and only if the combined quantum state $\hat{\rho}_{AB}$ can be written as

$$\hat{\rho}_{AB} = \sum_i p_i \hat{\rho}_A^i \otimes \hat{\rho}_B^i, \tag{1}$$

where $\{p_i\}$ corresponds to the probability distribution ($p_i \geqslant 0$ and $\sum_i p_i = 1$) and $\{\hat{\rho}_A^i\}$ and $\{\hat{\rho}_B^i\}$ are physical quantum states on subsystems A and B, respectively. Subsystems A and B are entangled if and only if they are not separable, i.e., their joint quantum state cannot be written in the form of Eq. (1).

The definition of quantum entanglement implies that when we consider any physical quantity on each subsystem, their joint property is the same as if we consider each subsystem as a separated state. For example, if we want to find the expectation value of $\langle \hat{x}_A \hat{x}_B \rangle$, the expectation values for the separable state becomes

$$\langle \hat{x}_A \hat{x}_B \rangle_{\hat{\rho}_{AB}} = \sum_i p_i \langle \hat{x}_A \rangle_{\hat{\rho}_A^i} \langle \hat{x}_B \rangle_{\hat{\rho}_B^i}, \tag{2}$$

which is simply the probabilistic mixture of the product of the expectation values on each subsystem.

Although this definition of quantum entanglement via inseparability is universal in a sense that it applies to any type of physical system, it is highly abstract and lacks any details, making it not so useful operationally. In this paper, we will restrict ourselves to the CV quantum entanglement.

III. NOTATIONS

In this section, we review the notation of the basic concepts and notations related to the CV optical system. When we consider the quantization of the electromagnetic field, we expand the electromagnetic field into a set of orthonormal *modes* (denoted with index k) and an annihilation operator (creation operator) $\hat{a}_k$ ($\hat{a}_k^\dagger$) associated with that mode. The superscript † is a Hermitian conjugate of an operator. The mode index k is associated with various properties that label the optical state we consider such as wavelength, polarization, temporal mode, spatial mode, and spectral distribution. The quantum states are then stored within modes. This is similar to classical electromagnetic field where we solve the Maxwell equations by expanding the basis in the orthonormal mode and find the values of the complex electromagnetic field amplitude associated with each mode. The annihilation and creation operators can be considered as quantum analogs to the classical complex electromagnetic field amplitude.

The annihilation and creation operators satisfy the following equation:

$$[\hat{a}_k, \hat{a}_{k'}^\dagger] = \delta_{kk'}, \tag{3}$$

which is the bosonic commutation relation. As the annihilation operators are not Hermitian operators, they are not the observable physical quantity. The quantity of our interest is the *quadrature* $\hat{x}_k$ and $\hat{p}_k$ which is given by[1]

$$\hat{x}_k = \sqrt{\frac{\hbar}{2}}(\hat{a}_k + \hat{a}_k^\dagger), \tag{4}$$

$$\hat{p}_k = -i\sqrt{\frac{\hbar}{2}}(\hat{a}_k - \hat{a}_k^\dagger). \tag{5}$$

These quantities can be considered to be equivalent to the real part and the imaginary part of the complex electric field amplitude. The quadrature amplitude can be easily measured using the measurement called homodyne measurement which is also a standard measurement in classical optics and telecommunication. In the CV system, we usually considered the quantum systems and their correlations from the aspect of the quadrature operators. Quantum states that have correlations in quadrature operators usually possess correlation in photon-number basis and they are useful for state generation [79], but for other applications such as quantum computation, quadrature-basis correlation is the main quantity of interest.

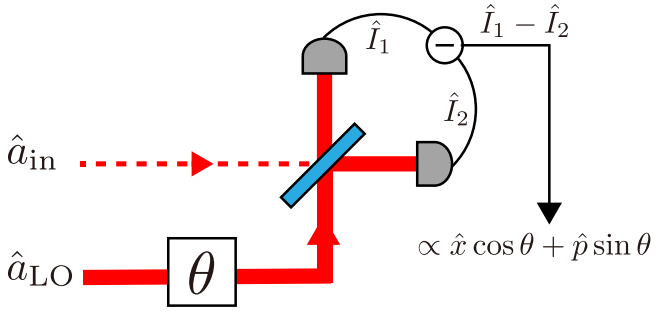

FIG. 1. Schematic diagram of the homodyne detector. The phase θ of the local oscillator determines the linear combination $\hat{x}\cos\theta + \hat{p}\sin\theta$ to be measured. The homodyne detector measures the difference of the current on the two photodiodes ($\hat{I}_1 - \hat{I}_2$).

We can easily show that the quadrature operators satisfy $[\hat{x}_k, \hat{p}_l] = i\hbar\delta_{kl}$, similar to the the position operator and momentum operator of a particle. From the commutation relation, we can show that the quadrature operators have the uncertainty principle given by

$$\langle \Delta^2 \hat{x} \rangle \langle \Delta^2 \hat{p} \rangle \geqslant \frac{\hbar^2}{4}, \tag{6}$$

$$\langle \Delta^2 \hat{x} \rangle + \langle \Delta^2 \hat{p} \rangle \geqslant \hbar, \tag{7}$$

where $\langle \Delta^2 \hat{x} \rangle = \langle \hat{x}^2 \rangle - \langle \hat{x} \rangle^2$ is the variance of the operator. The uncertainty principle plays an important role in the formulation of the concept of quantum entanglement and also the formulation of the criteria for detecting quantum entanglement.

Figure 1 shows the schematic of homodyne measurement. The homodyne detector amplifies the quadrature operator by interfering the quantum state with a strong classical light called local oscillator. The local oscillator also acts as a mode filtering; only the mode that is matched to the local oscillator is amplified and observable. The phase of the local oscillator determines the phase of the measured quadrature, allowing us to measure any arbitrary linear combination in a form of $\hat{x}\cos\theta + \hat{p}\sin\theta$, where θ is the phase of the local oscillator.

CV quantum states are usually grouped into two types: Gaussian states and non-Gaussian states. For pure states, they are categorized simply by whether the shapes of the Wigner functions are Gaussian or not. Although we can consider CV quantum entanglement for both Gaussian and non-Gaussian states, in this paper, we will restrict ourselves to the quantum entanglement in the Gaussian states. There are two reasons for this. The first reason is the experimental practicability. In the optical system, Gaussian states and Gaussian operations,

[1]Here we consider the case where $\omega = 1$ which holds in the case where the spectral of the quantum state of our interest is localized near the carrier frequency. This is the case that holds for almost all optical systems as their carrier frequencies are usually extremely high.

including multimode cases, are deterministic. This property makes generation of large-scale quantum entanglement via Gaussian toolbox highly appealing as there is no additional overhead from any probabilistic processes. The second reason is the simplicity in the analysis. If we consider a general quantum state of M mode where each mode is truncated to a max photon number N, then the parameters required to uniquely describe the state are typically on the order of N^M. On the other hand, for Gaussian states, although Gaussian states are usually not truncated in photon-number basis, they can be uniquely determined (up to displacement) with a covariance matrix (see Sec. IV). This means that describing Gaussian states, regardless of the photon number, requires only $(2M)^2$ parameters. We see that the scaling in M is exponential in the general case, while it is only square in the Gaussian case. This makes characterization of multimode Gaussian states more viable compared to general multimode quantum states.

Now let us define Gaussian operations and Gaussian states. Here we will restrict ourselves to the case of the pure states. For a detailed review on the Gaussian toolbox of CV quantum computation, see Ref. [80] for a review. The Gaussian operations transform Gaussian states to other Gaussian states. In the Heisenberg picture, Gaussian operations can be written as

$$\hat{\mathbf{q}}' = \mathbf{S}\hat{\mathbf{q}} + \mathbf{q}_0, \tag{8}$$

where the hat vector is

$$\hat{\mathbf{q}}' = \begin{pmatrix} \hat{x}_1 \\ \hat{x}_2 \\ \vdots \\ \hat{x}_N \\ \hat{p}_1 \\ \hat{p}_2 \\ \vdots \\ \hat{p}_N \end{pmatrix}. \tag{9}$$

Because the transformation of the quadrature must preserve the commutation relation, the matrix $\mathbf{S}$ must be a symplectic matrix satisfying

$$\mathbf{S}\Omega\mathbf{S}^{\mathrm{T}} = \Omega \tag{10}$$

with

$$\Omega = \begin{pmatrix} \mathbf{0} & \mathbf{I} \\ -\mathbf{I} & \mathbf{0} \end{pmatrix}. \tag{11}$$

A. Single-mode Gaussian operations

In this subsection, we will briefly cover basic single-mode Gaussian operations

1. Displacement operation

The displacement operation corresponds to the scalar part in Eq. (8). As we will see in Sec. V, the CV quantum entanglements are defined by the linear correlation of the quadrature operators, meaning that the displacement operations are trivial as they are simply redefining the offset of the quadrature values.

2. Phase rotation

Phase rotation $\hat{R}(\theta)$ of the quadrature operators can be written as

$$\begin{pmatrix} \hat{x}' \\ \hat{p}' \end{pmatrix} = \mathbf{R}(\theta)\begin{pmatrix} \hat{x} \\ \hat{p} \end{pmatrix} = \begin{pmatrix} \cos\theta & -\sin\theta \\ \sin\theta & \cos\theta \end{pmatrix}\begin{pmatrix} \hat{x} \\ \hat{p} \end{pmatrix}, \tag{12}$$

which corresponds to the rotation in the phase space. In the optical system, phase rotation can be realized by simply changing the optical path length that the state propagates.

3. Squeezing operation

The squeezing operation $\widehat{Sq}(r)$ is given by

$$\begin{pmatrix} \hat{x}' \\ \hat{p}' \end{pmatrix} = \mathbf{Sq}(r)\begin{pmatrix} \hat{x} \\ \hat{p} \end{pmatrix} = \begin{pmatrix} e^r & 0 \\ 0 & e^{-r} \end{pmatrix}\begin{pmatrix} \hat{x} \\ \hat{p} \end{pmatrix}. \tag{13}$$

Squeezing operation is a basic component in the generation of optical quantum entanglement, and is usually the only nonlinear optics process required in the entanglement generation. Experimentally, rather than implementing squeezing operation directly on quantum states, we usually generate squeezed vacuum states (i.e., a vacuum state that has squeezing operation acting on it, also simply called a squeezed state) and use them as our initial resources.

B. Two-mode Gaussian operations

In this subsection, we will briefly cover the basic two-mode Gaussian operations.

1. Controlled-Z gate

The unitary operator of the controlled-Z gate is given by

$$\hat{C}_Z(g) = \exp\left(\frac{i}{\hbar} g\hat{x}_1 \otimes \hat{x}_2\right), \tag{14}$$

where g is the gain that is tunable. This operation transforms the quadrature operator as follows:

$$\begin{pmatrix} \hat{x}_1' \\ \hat{x}_2' \\ \hat{p}_1' \\ \hat{p}_2' \end{pmatrix} = \begin{pmatrix} 1 & 0 & 0 & 0 \\ 0 & 1 & 0 & 0 \\ 0 & g & 1 & 0 \\ g & 0 & 0 & 1 \end{pmatrix}\begin{pmatrix} \hat{x}_1 \\ \hat{x}_2 \\ \hat{p}_1 \\ \hat{p}_2 \end{pmatrix}. \tag{15}$$

As we can see, interaction from controlled-Z gate mixes the p quadrature with the x quadrature operator from the other mode. Controlled-Z gate is a popular type of interaction usually used in the early theoretical calculations regarding CV quantum entanglement and measurement-based quantum computation [81]. This is because controlled-Z gate affects only single quadrature and has nice parallelism to the entangling gate in the qubit system. Optical realization of the controlled-Z gate was implemented using linear optics and squeezing gate [82,83] as they come naturally in the optical system.

2. Beam-splitter interaction

Although the controlled-Z gate suffices as the two-mode interaction, a more widely used interaction in the optical system is the beam-splitter interaction. Implementation of the beam-splitter interaction is very straightforward in the optical

regime; we simply put a coated plate of glass and then interfere two beams at that glass. Without the loss of generality, the beam-splitter interaction transforms the quadrature operators in the Heisenberg picture as

$$\begin{pmatrix} \hat{x}_1' \\ \hat{x}_2' \\ \hat{p}_1' \\ \hat{p}_2' \end{pmatrix} = \begin{pmatrix} \sqrt{R} & -\sqrt{T} & 0 & 0 \\ \sqrt{T} & \sqrt{R} & 0 & 0 \\ 0 & 0 & \sqrt{R} & -\sqrt{T} \\ 0 & 0 & \sqrt{T} & \sqrt{R} \end{pmatrix} \begin{pmatrix} \hat{x}_1 \\ \hat{x}_2 \\ \hat{p}_1 \\ \hat{p}_2 \end{pmatrix}, \tag{16}$$

with $R + T = 1$, where R and T correspond to the energy reflectivity and transmittivity of the beam splitter, respectively. We can see that the beam-splitter interaction defined here does not mix the two quadratures x and p. We can also make a beam-splitter interaction that mixes the quadrature, but that is equivalent to adding additional phase rotation to Eq. (16). Unlike the controlled-Z gate, the beam-splitter interaction changes both quadratures which could make their visualization more difficult than controlled-Z gate (see Sec. IV B). Availability of the easy-to-use beam-splitter interaction is one of the main factors that makes generation and manipulation of the quantum entanglement much developed in the optical systems.

C. Gaussian decomposition

We have discussed various basic Gaussian gates. Next let consider how to construct a Gaussian operation when a symplectic matrix $\mathbf{S}$ of the desired operation is given. As any Gaussian operations are uniquely determined (up to displacement operation) by their symplectic matrix, the problem of constructing a Gaussian operation is equivalent to the decomposition problem of the symplectic matrix. One of the useful decompositions of the symplectic matrix is called the Bloch-Messiah decomposition [84,85] which decomposes arbitrary symplectic matrix $\mathbf{S}$ into

$$\mathbf{S} = \mathbf{O} \begin{pmatrix} \mathbf{\Lambda}^{-1} & \mathbf{0} \\ \mathbf{0} & \mathbf{\Lambda}^{1} \end{pmatrix} \mathbf{O}', \tag{17}$$

where $\mathbf{O}$ and $\mathbf{O}'$ are orthogonal and symplectic, and Λ is a diagonal matrix whose elements are all positive. Although we have not explicitly stated it, the symplectic transform that is also orthogonal matrix corresponds to the passive linear optics network composed of beam splitters and phase rotations. On the other hand, the $\mathbf{\Lambda}$ part corresponds to a single-mode squeezing. Therefore, we can decompose any arbitrary Gaussian operation into linear optics network and single-mode squeezing.

Another useful decomposition of the symplectic matrix is [86]

$$\mathbf{S} = \begin{pmatrix} \mathbf{I} & \mathbf{0} \\ \mathbf{V} & \mathbf{I} \end{pmatrix} \begin{pmatrix} \mathbf{U}^{-1/2} & \mathbf{0} \\ \mathbf{0} & \mathbf{U}^{1/2} \end{pmatrix} \mathbf{O}'', \tag{18}$$

where $\mathbf{O}''$ is an orthogonal matrix, $\mathbf{U}$ and $\mathbf{V}$ are both symmetric matrices, with only $\mathbf{U}$ being positive definite. Although decomposition in Eq. (18) is similar to Eq. (17), the leftmost matrix resembles the controlled-Z gate, while for the middle matrix, although it has some resemblance to the $\mathbf{\Lambda}$, it is not orthogonal, thus does not directly correspond to squeezing operation

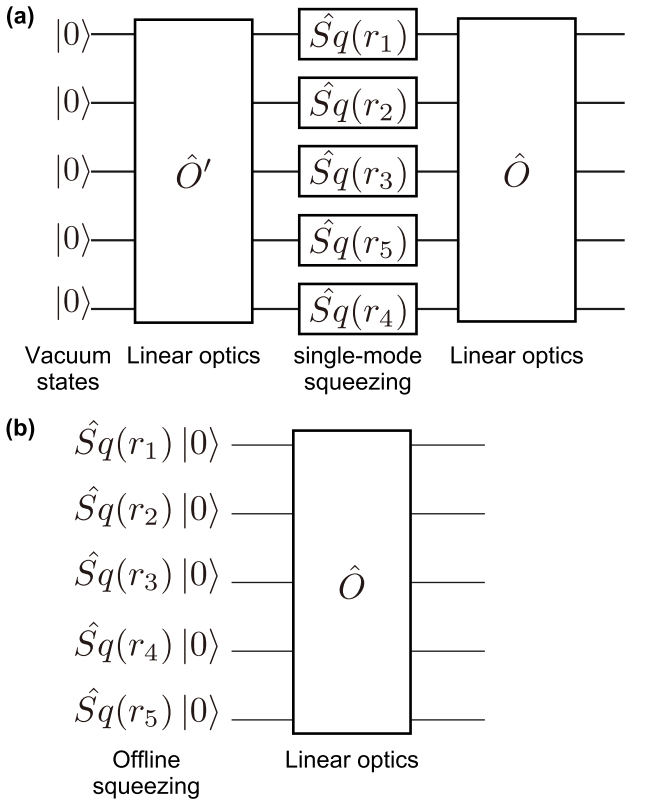

FIG. 2. Generation of arbitrary Gaussian states from vacuum states. The example here shows the case of five-mode Gaussian state. (a) Generation circuit based on the Bloch-Messiah decomposition. (b) Equivalent circuit based on offline squeezed states and linear optics. $\hat{O}$ and $\hat{O}'$ are linear optics operation which are not unique as Bloch-Messiah decomposition is not a unique decomposition. $\widehat{Sq}(r)$ is a squeezing operation.

IV. MULTIMODE GAUSSIAN STATES

In this section, we will define multimode Gaussian states and how to represent them. Pure Gaussian state is a quantum state whose wave function is a (complex) Gaussian function. If we represent the state in the phase space using the Wigner function, the Wigner function becomes a real Gaussian function. In fact, a quantum pure state is Gaussian if and only if it has no negative region in its Wigner function [87].

Figure 2 shows how to generate an arbitrary multimode Gaussian state. If we can implement arbitrary Gaussian operations, then any pure N-mode Gaussian states can be generated by applying Gaussian operations to N-mode vacuum state. Using the decomposition in Eq. (17) and the fact that beam-splitter interaction on vacuum states results in vacuum states, we can readily show that arbitrary N-mode Gaussian states can be generated by combining N single-mode squeezed vacuum states on a linear optics network. This is an important result in CV optical system as generation of a squeezed vacuum state is much simpler than applying squeezing operation on an arbitrary quantum state [88,89].

A. Representation of Gaussian states

In this section, we will discuss different ways of defining Gaussian states, thus the CV quantum entanglement.

1. Wave function and Wigner function

First let us consider how to derive the wave function of the single-mode vacuum state. The single-mode vacuum state $|0\rangle$ satisfies

$$\hat{a}|0\rangle = \frac{\hat{x} + i\hat{p}}{\sqrt{2\hbar}}|0\rangle = 0. \tag{19}$$

To find the wave function $\psi_0(x) = \langle x|0\rangle$, we put bra $\langle x|$ on the left side of Eq. (19) and do the change $\hat{x} \to x$ and $\hat{p} \to -i\hbar\frac{\mathrm{d}}{\mathrm{dx}}$ which gives the equation

$$\left(x + \hbar\frac{d}{dx}\right)\psi_0(x) = 0. \tag{20}$$

This gives

$$\psi_0(x) = N \exp\left(-\frac{x^2}{2\hbar}\right), \tag{21}$$

where N is a normalization factor. Now let us consider an N-mode Gaussian state $|\psi_G\rangle$ that is connected to $|0\rangle$ via a Gaussian operation $\hat{U}_G$. Then, from Eq. (19), we can show that this state must satisfy

$$\hat{U}_G\hat{\mathbf{a}}\hat{U}_G^\dagger|\psi_G\rangle = \mathbf{0}, \tag{22}$$

where $\hat{\mathbf{a}} = (\hat{a}_1\ \hat{a}_2\ \ldots\ \hat{a}_N)^{\mathrm{T}}$ is a vector of annihilation operator for each mode and the above equation is a shorthand for N equations. Note also that in our notation the transpose of the vector of the operator does not transpose the operator inside. As the transformation of $\hat{\mathbf{a}}$ is an inverse of the transformation of the operators in the Heisenberg picture, the transformation here is done by the inverse of $\mathbf{S}$. Using the form of $\mathbf{S}$ in Eq. (18) and the fact that beam-splitter interaction on vacuum does not do anything, we put $\mathbf{O}'' = \mathbf{I}$ and find $\mathbf{S}^{-1}$ as

$$\begin{aligned}\mathbf{S}^{-1} &= \begin{pmatrix}\mathbf{U}^{1/2} & 0\\ 0 & \mathbf{U}^{-1/2}\end{pmatrix}\begin{pmatrix}\mathbf{I} & 0\\ -\mathbf{V} & \mathbf{I}\end{pmatrix}\\ &= \begin{pmatrix}\mathbf{U}^{1/2} & 0\\ -\mathbf{U}^{-1/2}\mathbf{V} & \mathbf{U}^{-1/2}\end{pmatrix}.\end{aligned} \tag{23}$$

Then, we get the new equation as

$$[(\mathbf{U}^{1/2} - i\mathbf{U}^{-1/2}\mathbf{V})\hat{\mathbf{x}} + i\mathbf{U}^{-1/2}\hat{\mathbf{p}}]|\psi_G\rangle = \mathbf{0}, \tag{24}$$

$$[(\mathbf{U} - i\mathbf{V})\hat{\mathbf{x}} + i\hat{\mathbf{p}}]|\psi_G\rangle = \mathbf{0}. \tag{25}$$

Doing the same substitution as Eq. (20), we arrive at

$$\psi_G(x) = N_G \exp\left[-\frac{1}{2\hbar}\mathbf{x}^{\mathrm{T}}(\mathbf{U} - i\mathbf{V})\mathbf{x}\right]. \tag{26}$$

Thus, the property of the wave function is determined by the combination of $\mathbf{U}$ and $\mathbf{V}$ which has been shown to be related to the graphical representation of the multimode Gaussian states [90] (see Sec. IV B).

Next let us look at the Wigner function representation of the multimode Gaussian states. There are many different ways to define the Wigner function. For our purpose, let us use the following definition:

$$W(\mathbf{q}) = \frac{1}{\pi\hbar}\mathrm{Tr}[(-1)^{\hat{N}}\hat{D}(-\mathbf{q})\hat{\rho}\hat{D}^\dagger(-\mathbf{q})], \tag{27}$$

where $\hat{N} = \sum_i \hat{n}_i$ is the sum of the photon in all modes with $\hat{n}_i$ being a photon-number operator in mode i. This equation means that the value of the Wigner function at coordinate $\mathbf{q} = \binom{\mathbf{x}}{\mathbf{p}}$ is equal to the parity at that point. When $\hat{\rho}$ is acted on with Gaussian operation $\hat{U}_G$, by using the relation between Gaussian operation and displacement operator, and the fact that $(-1)^{\hat{N}}$ is a π phase shift, we have

$$\begin{aligned}W_{\hat{U}_G}(\mathbf{q}) &= \frac{1}{\pi\hbar}\mathrm{Tr}[(-1)^{\hat{N}}\hat{D}(-\mathbf{S}^{-1}\mathbf{q})\hat{\rho}\hat{D}^\dagger(-\mathbf{S}^{-1}\mathbf{q})]\\ &= W_{\hat{\rho}}(\mathbf{S}^{-1}\mathbf{q}).\end{aligned} \tag{28}$$

This means that Gaussian operation corresponds to linear coordinate transformation of the Wigner function.

2. Covariance matrix

Another way to uniquely determine a pure Gaussian state is via the covariance matrix. Let us define the covariance matrix $\mathbf{C}$ as

$$\mathbf{C} = \tfrac{1}{2}\langle\hat{\mathbf{q}}\hat{\mathbf{q}}^{\mathrm{T}} + (\hat{\mathbf{q}}\hat{\mathbf{q}}^{\mathrm{T}})^{\mathrm{T}}\rangle. \tag{29}$$

Using Eq. (18), we can readily calculate this as

$$\mathbf{C} = \frac{\hbar}{2}\begin{pmatrix}\mathbf{U}^{-1} & \mathbf{U}^{-1}\mathbf{V}\\ \mathbf{V}\mathbf{U}^{-1} & \mathbf{U} + \mathbf{V}\mathbf{U}^{-1}\mathbf{V}\end{pmatrix}. \tag{30}$$

We see that when $\mathbf{V} = 0$ there is no correlation between quadrature x and p.

B. Graphical representation

As we have seen, Gaussian states are characterized by the complex combination $\mathbf{U} - i\mathbf{V}$ which is a symmetric matrix. In Ref. [90], it has been shown that by considering a matrix

$$\mathbf{Z} = \mathbf{V} + i\mathbf{U}, \tag{31}$$

multimode Gaussian states could be represented as a graph where matrix $\mathbf{Z}$ is a matrix of the complex edge weight between modes. Gaussian transformations can also be rewritten as the transformation of graph which affected only the edge weights of the edges that are connected to the modes that are operated on. In this paper, we will not go into the details of the graphical calculus, and the readers should consult Ref. [90] for more details if necessary. With graphical calculus, all the graphical representations of the entanglement in this paper are not just schematic diagrams but are equivalent to actual mathematical descriptions of states.

Graphical calculus is an important tool in describing large-scale quantum entanglement. The reason for this is not only because graphical calculus allows us to visualize the entanglement, but also due to the fact that describing entangled states using equations becomes unrealistic when the number of the modes greatly increases. Moreover, graphical calculus lets us describe the change of the entangled state via graphical transformation rules without having to resort to mathematical

equations. This is convenient when we want to describe the effects of gates or measurements on modes of the entangled state. Another instance that makes graphical calculus highly useful is the fact that large-scale optical entanglement is usually generated in the manner that its graphical structure is periodical. Thus, we can look at a small number of nodes in the graphical structure and infer the structure and relation of the whole entangled state.

V. MULTIMODE CONTINUOUS-VARIABLE ENTANGLEMENT

A. Entanglement and finite squeezing

As the first example of the entangled state, we consider the case of two-mode entangled state. In this case, the most well-known state is the Einstein-Podolsky-Rosen (EPR) state which first appeared in the paper by the authors of the same name [12].

One of the ways to think about the EPR state is that although $\hat{x}$ and $\hat{p}$ do not commute, the linear combination could commute:

$$[\hat{x}_1 - \hat{x}_2, \hat{p}_1 + \hat{p}_2] = 0. \tag{32}$$

This means that quantum mechanics allows such a state which is a simultaneous eigenstate of $\hat{x}_1 - \hat{x}_2$ and $\hat{p}_1 + \hat{p}_2$.

Now comes what makes the CV system more complicated than the qubit system; although these states are allowed, it does not mean that these states are physical. One could naively try to write the EPR state as

$$|\psi_{\mathrm{EPR}}\rangle = \int dx\, |x\rangle_1 |x\rangle_2 = \int dp\, |p\rangle |-p\rangle. \tag{33}$$

Note that the representation between $\hat{x}$ and $\hat{p}$ basis stems from

$$|p\rangle = \frac{1}{\sqrt{2\pi\hbar}} \int dx\, \exp\left(\frac{i}{\hbar} xp\right) |x\rangle. \tag{34}$$

$|\psi_{\mathrm{EPR}}\rangle$, however, obviously does not represent a physical state. This is a recurring difficulty in the CV system. In most of the cases, the entanglements we wish to generate for some particular applications are sought for their correlation in the quadrature operators. However, when one tries to write the state, we found that the state is unphysical.

Even if the state we want is unphysical, experimentally, we can think of how to approximate the state. This way of thinking is similar to how the x eigenstate is usually approximated by the x-squeezed state in the experiment as the variance in x and p of the x-squeezed state approaches the same value as the x eigenstate when the squeezing level is taken to infinite limit. Thus, we can try to approximate the quantum entangled state by finding the state whose correlation we want approaches an ideal value when the squeezing level is taken to infinite limit

Here we emphasize that it is important not only to consider the realistic finite-squeezing case, but also the infinite-squeezing limit when we build an experimental setup. It is not difficult to come up with a system that, although it does not give the desired quantum correlation in the infinite-squeezing asymptotic limit, the correlation level at certain squeezing level could be better than the classical correlation. This, however, does not necessarily make the setup appropriate for approximating the target state as the state generated does not converge to the target state at the infinite-squeezing limit.

B. Nullifiers

Following the idea of the last section, we can consider the nullifiers. For N-mode Gaussian state $|\psi_N\rangle$, the nullifier $\hat{\delta}_i$ is an operator that satisfies

$$\hat{\delta}_i |\psi_N\rangle = 0. \tag{35}$$

The state $|\psi_N\rangle$ can be specified by N linearly independent and commutative nullifiers, and there is a one-to-one correspondence between the state and the nullifier. As an example, the nullifiers of the EPR state are $\hat{x}_1 - \hat{x}_2$ and $\hat{p}_1 + \hat{p}_2$. Linear combinations of the nullifiers are also nullifiers, and we can consider the transformation of the nullifiers when unitary transformation $\hat{U}$ acts on the state as

$$\hat{\delta} \to \hat{U} \hat{\delta} \hat{U}^\dagger \tag{36}$$

which is the inverse of the transformation in the Heisenberg picture.

For a state with finite squeezing, Eq. (36) gives the form of the nullifiers for arbitrary multimode Gaussian states and entanglement as arbitrary Gaussian states can be generated by applying Gaussian operations to vacuum state.

The issue with Eq. (36) is that the annihilation operator is not an observable. It would be much more convenient to start from the state that has quadrature operators as their nullifiers (such as quadrature eigenstate) because the resulting state will be nullified by linear combination of quadrature operators which are measurable. Similar to the EPR state, however, these ideal states are usually unnormalizable making their state vector representation difficult to be related to experiment. On the other hand, when the ideal nullifiers are given, it is of experimental interest to find the ways to produce the state that approaches the ideal state in the limit of infinite squeezing. For a type of state called cluster state, this has been exhaustively explored and we will discuss this in Sec. V D 1.

Then, it is the question of interest of how to find a system that approximates the desired states that are defined by the nullifiers. To look at this, let us consider nullifiers of N-mode entanglement in the form

$$\hat{\boldsymbol{\delta}} = (\mathbf{A} \quad \mathbf{B}) \begin{pmatrix} \hat{\mathbf{x}} \\ \hat{\mathbf{p}} \end{pmatrix}, \tag{37}$$

where $\mathbf{A}$ and $\mathbf{B}$ are $N \times N$ real matrices. As we are considering a set of nullifiers that uniquely determines the state, all nullifiers must be commutable, i.e., $[\hat{\delta}_i, \hat{\delta}_j] = 0$ for all i, j. From the form of $\hat{\boldsymbol{\delta}}$, we can compactly write the condition as

$$\mathbf{A}\mathbf{B}^{\mathrm{T}} - \mathbf{B}\mathbf{A}^{\mathrm{T}} = \mathbf{0}. \tag{38}$$

The above condition must be satisfied for the simultaneous eigenstate of the assigned set of nullifiers to be allowed (even though they are not necessarily physical). To consider actual generation system, let us consider the singular value decomposition of $(\mathbf{A} \quad \mathbf{B})$

$$(\mathbf{A} \quad \mathbf{B}) = \mathbf{O}_{N\times N} \boldsymbol{\Sigma}_{N\times 2N} \mathbf{O}'^{\mathrm{T}}_{2N\times 2N}, \tag{39}$$

where the lower indices indicate the dimension of each matrix. $\mathbf{O}$ and $\mathbf{O}'$ are orthogonal matrices, while $\boldsymbol{\Sigma}$ is a diagonal

rectangular matrix with non-negative elements. From the linear independency $\text{rank}(\mathbf{\Sigma}) = N$, so all diagonals of $\mathbf{\Sigma}$ are nonzero. Note that typical singular value decomposition only requires that the diagonals of $\boldsymbol{\sigma}$ to be non-negative, and the nonzero requirements come from independency assumption. Inserting Eq. (39) into (37), we have

$$\hat{\boldsymbol{\delta}} = \mathbf{O}\mathbf{\Sigma}\mathbf{O}'^{\mathrm{T}}\hat{\mathbf{q}}. \tag{40}$$

As the orthogonal matrix $\mathbf{O}$ corresponds to linear combination of the nullifiers, it does not affect the actual nullifiers and can be canceled out. The matrix $\mathbf{\Sigma}$ is also multiplication of constant value on each nullifier; this can also be ignored, so we have

$$\hat{\boldsymbol{\delta}} = (\mathbf{I} \quad \mathbf{0})\mathbf{O}'^{\mathrm{T}}\hat{\mathbf{q}}. \tag{41}$$

As $\mathbf{O}'^{\mathrm{T}}$ is an inverse of the linear optics given by $\mathbf{O}'$ and $(\mathbf{I} \quad \mathbf{0})\hat{\mathbf{q}} = \hat{\mathbf{x}}$ is simply the nullifier of the x eigenstate, the state given by nullifiers that is linear combination of quadrature operators can be realized simply by combining x-squeezed states on a linear optics determined by $\mathbf{O}'$. Note that the linear optics for realizing particular nullifiers is not unique as we can add linear optics that do not change x-squeezed state as much as we want. In Ref. [75], the network for realizing arbitrary cluster state with offline squeezing and linear optics was demonstrated by canceling the antisqueezing component in the nullifiers.

C. Figure of merit and criteria for quantum entanglement

Next, let us consider how to evaluate the CV optical quantum entanglement. For Gaussian states, measuring the covariance matrix uniquely defines the states. From the covariance matrix, figures of merit such as fidelity, purity, and various entanglement indicators can be calculated. We will not go into the details here and let the reader consult Ref. [80]. For evaluation of large-scale quantum entanglement such as one-million-mode quantum entanglement in Ref. [52], however, the covariance matrix becomes difficult to handle, and not necessarily relevant when considering the applications with large-scale entanglement.

The early sufficient criteria for checking the existence of quantum entanglement were put out by Horodecki [91]. The criteria proposed were based on the positivity of the partial transpose operation on the separable state. In 2000, a separate work by Duan [92] and Simon [93] has extended the criteria by Horodecki into a necessary and sufficient criteria for determining whether there is entanglement between the two-mode states. Their formulations are based on quadratures and covariance matrix which can be easily measured experimentally. Later, these criteria were extended to sufficient criteria for the multimode case by van Loock and Furusawa [94] and have become a standard tool for evaluation of large-scale optical CV quantum entanglement.

Before going into the details of van Loock–Furusawa (vLF) criteria, let us discuss why vLF criteria are useful for evaluating quantum entanglement. vLF criteria utilize the fact that for the separable state, quadrature correlations will have a lower limit. Although we are free to select the form of the correlation, it is usually advantageous to use nullifiers as they approach 0 for ideal states. Moreover, as large-scale entanglement generated with multiplexing usually has periodic graphical structure, applying the measured correlation to vLF criteria is simple, even when the number of modes becomes extremely large. When used in quantum protocol such as quantum teleportation or computation, the variances of the nullifiers are usually directly equal to the intrinsic squeezing noise. Hence, vLF criteria utilize the physical quantities that are directly related to quantum protocol.

Even if the states are the same in the asymptotic infinite-squeezing limit, in the finite-squeezing limit, the variances can be dependent on how the state is generated. In the case of the generation using linear optic and offline squeezing (where all the squeezing levels are assumed to be equal), decomposition in Eq. (17) and the form of nullifiers in Eq. (41) suggests that the variances of the nullifiers will squeeze below vacuum equal to the squeezing level of the initial resources. This is because when linear optics are applied to vacuum state input, the output is simply a vacuum state without any changes. On the other hand, if we use, for example, controlled-Z gate and squeezed state for the generation, the variance of the nullifiers will be different as controlled-Z gate generates entanglement even if the vacuum inputs are used. One way to reconcile this is to notice that controlled-Z gate has squeezer in it when we do Bloch-Messiah decomposition [88].

In vLF criteria, we consider operators that are linear in the quadrature which are given by

$$\hat{\xi} = \sum_{k\in\mathcal{A}}(g_k\hat{x}_k + h_k\hat{p}_k) + \sum_{l\in\mathcal{B}}(g_l\hat{x}_l + h_l\hat{p}_l), \tag{42}$$

$$\hat{\zeta} = \sum_{k\in\mathcal{A}}(g'_k\hat{x}_k + h'_k\hat{p}_k) + \sum_{l\in\mathcal{B}}(g'_l\hat{x}_l + h'_l\hat{p}_l), \tag{43}$$

where g_k, g'_k, h_k, h'_k are real numbers and we have grouped the mode indices into two sets $\mathcal{A}$ and $\mathcal{B}$ where $\mathcal{A}\cap\mathcal{B} = \phi$. Note that we restrict the coefficients to be real so that the operators $\hat{\xi}$ and $\hat{\zeta}$ are observable. In principle, for the purpose of vLF criteria, these operators do not have to commute or correspond to nullifiers of the state. We will see, however, that for practical purposes in the verification of large-scale quantum entanglement, selecting $\hat{\xi}$ and $\hat{\zeta}$ to be nullifiers has many advantages.

Next, we consider a quantum state that is separable with respect to $\mathcal{A}$ and $\mathcal{B}$, i.e.,

$$\hat{\rho}_{\mathcal{AB}} = \sum_i p_i\hat{\rho}^i_{\mathcal{A}}\otimes\hat{\rho}_{\mathcal{B}}. \tag{44}$$

$\hat{\rho}_{\mathcal{A}}$ is a quantum state on the subsystem defined by $\mathcal{A}$ and so on. If we measure the variances of $\hat{\xi}$ and $\hat{\zeta}$, we can easily show that [94]

$$\langle\Delta^2\hat{\xi}\rangle_{\hat{\rho}_{\mathcal{AB}}} + \langle\Delta^2\hat{\zeta}\rangle_{\hat{\rho}_{\mathcal{AB}}} = \sum_i p_i\big[\langle\Delta^2\hat{\xi}_{\mathcal{A}}\rangle_{\hat{\rho}^i_{\mathcal{A}}} + \langle\Delta^2\hat{\zeta}_{\mathcal{A}}\rangle_{\hat{\rho}^i_{\mathcal{A}}} + \langle\Delta^2\hat{\xi}_{\mathcal{B}}\rangle_{\hat{\rho}^i_{\mathcal{B}}} + \langle\Delta^2\hat{\zeta}_{\mathcal{B}}\rangle_{\hat{\rho}^i_{\mathcal{B}}}\big], \tag{45}$$

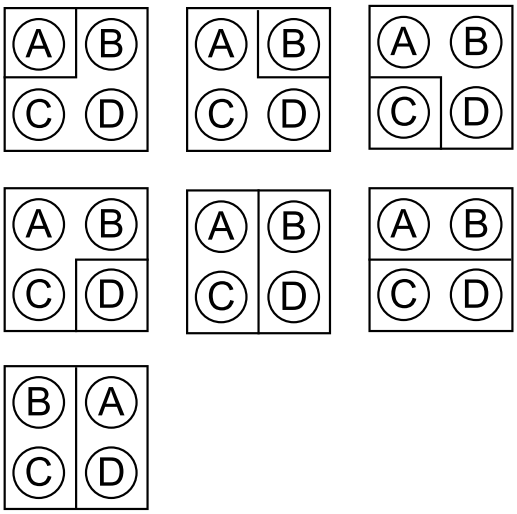

FIG. 3. Bipartitions of four-partite state. Negating all of these possible configurations establishes genuine multipartite inseparability.

where the variance is defined as $\langle \Delta^2 \hat{x} \rangle = \langle \hat{x}^2 \rangle - \langle \hat{x} \rangle^2$ and the definition of each operator is

$$\hat{\xi}_{\mathcal{A}} = \sum_{k \in \mathcal{A}} (g_k \hat{x}_k + h_k \hat{p}_k), \tag{46}$$

$$\hat{\zeta}_{\mathcal{A}} = \sum_{k \in \mathcal{A}} (g'_k \hat{x}_k + h'_k \hat{p}_k), \tag{47}$$

$$\hat{\xi}_{\mathcal{B}} = \sum_{l \in \mathcal{B}} (g_l \hat{x}_l + h_l \hat{p}_l), \tag{48}$$

$$\hat{\zeta}_{\mathcal{B}} = \sum_{l \in \mathcal{B}} (g'_l \hat{x}_l + h'_l \hat{p}_l). \tag{49}$$

Invoking the uncertainty principle [Eq. (7)], we arrive at

$$\langle \Delta^2 \hat{\xi} \rangle_{\hat{\rho}_{\mathcal{AB}}} + \langle \Delta^2 \hat{\zeta} \rangle_{\hat{\rho}_{\mathcal{AB}}} \geqslant \hbar \left(\left| \sum_{k \in \mathcal{A}} g_k h'_k - g'_k h_k \right| + \left| \sum_{l \in \mathcal{B}} g_l h'_l - g'_l h_l \right| \right). \tag{50}$$

Equation (50) means that if we measure the variances of $\hat{\xi}$ and $\hat{\zeta}$ and find that they are below a threshold determined by the right side of Eq. (50), then we can establish that the state is inseparable with respect to $\mathcal{A}$ and $\mathcal{B}$. By selecting appropriate operators, we can negate the possibility of the state being in any biseparable form, which leads to the conclusion that the state is inseparable. For example, if we want to show that a four-partite state is inseparable, we have to use vLF criteria to negate the possibility of seven types of biseparable form shown in Fig. 3. This equation is the van Loock–Furusawa criteria [94]. Note that in the original paper, they only considered the form where there are only x or p quadratures in the linear combination.

The fact that vLF criteria utilize variances makes them highly compatible with the nullifiers as the nullifiers approach zero when the entanglement approaches ideal form. From the experimental point of view, there are also other considerations that need to be taken into account.

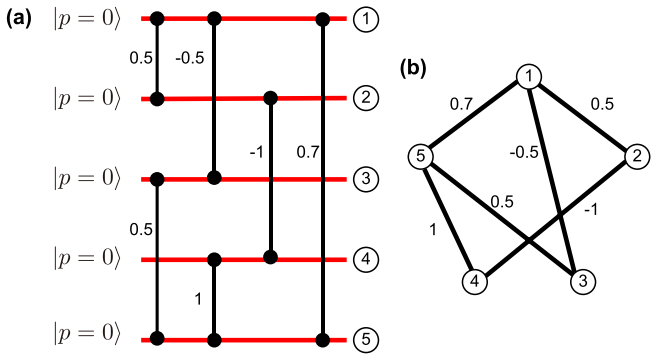

FIG. 4. Cluster states generated from controlled-Z gate. (a) A particular circuit for state generation. The black line corresponds to controlled-Z gate and the number is the gain g. (b) Corresponding graphical representation determined by the adjacency matrix $\mathcal{A}$.

D. Examples of CV entanglement

In this section, we will give some examples of the common CV quantum entanglement.

1. Cluster state

The first type of the state is called the cluster state. The cluster state is a resource for measurement-based quantum computation [81,95]. Traditionally, the cluster state is defined via p eigenstate, controlled-Z gate, and adjacency matrix $\mathcal{A}$ as

$$|\psi_{\mathcal{A}}\rangle = \hat{C}_Z[\mathcal{A}]|p=0\rangle^{\otimes N}, \tag{51}$$

$$\hat{C}_Z[\mathcal{A}] = \exp\left(\frac{i}{2\hbar} \hat{\mathbf{x}}^{\mathrm{T}} \mathcal{A} \hat{\mathbf{x}}\right). \tag{52}$$

Figure 4 shows an example of cluster state generated in this manner. In this definition, the matrix $\mathcal{A}$ directly corresponds to the graphical representation of the state, i.e., $\mathbf{Z} = \mathcal{A}$ in Eq. (31), which makes the graphical representation of this type of the state easy to write. The nullifier for this type of state also becomes $\hat{\boldsymbol{\delta}} = \hat{\mathbf{p}} - \mathcal{A}\hat{\mathbf{x}}$.

Despite the simplicity in the definition and a strong parallelism to the qubit cluster state, straightforward generation based on the controlled-Z gate is difficult in the optical system as it is not a naturally available interaction. Although there is experimental demonstration of the controlled-Z gate using linear optics and measurement-induced squeezing gates [82,83], the system is too complex to be repeated several times. There is an early theoretical proposal that uses time multiplexing with the controlled-Z gate to realize a scalable cluster state [39], but even then a single controlled-Z gate remains challenging and resource inefficient due to the additional ancillary state. A better approach is via linear optics and offline squeezing as explained in Sec. IV. Based on this approach, small-scale cluster states with many different structures have been realized [23–32] and even some demonstrations of applications using these cluster states also have been demonstrated.

There are, however, a few experimental hurdles for this approach. First, in addition to the structure, the linear optics required for the state generation is highly dependent on the mode number N. If we were to use the generation via

the controlled-Z gate as in Eq. (52), then adding the mode is a simple task as all controlled-Z gates commute. On the other hand, the structure of the linear optics for the generation with offline squeezing depends on the decomposition of $\mathcal{A}$ as shown in Eq. (17) which in general would be very dependent on the dimension of the matrix. Moreover, unlike the controlled-Z gate, beam-splitter interactions in general do not commute. There is a recent work that utilizes variable beam splitter and loop structure to circumvent this limitation [96], but even then generation of large-scale entanglement with this approach is not easy and there are other approaches that can be taken. Experimentally, the p eigenstates are approximated using p-squeezed state as the quadrature distribution of p-squeezed state bears more resemblance to the p eigenstate as the squeezing level increases [97].

Another problem with this definition of cluster state is that they cannot incorporate the quantum entanglement that is related to the cluster state but are not exactly of this type. For example, it can be easily shown that the EPR state in Sec. V A is related to two-mode linear cluster state via $\pi/2$ phase shift of one mode. In the recent experimental generation of large-scale cluster state, the "cluster state" does not have the form defined in Eq. (52), but is usually related to it via local phase rotation [90]. This difference does not affect any capability of the state in the quantum computation as local phase rotation simply means that measurement bases can just be redefined when the state is used.

2. $\mathcal{H}$-graph state

A type of entanglement that is highly related to the cluster state is called the $\mathcal{H}$-graph state. In fact, many of the generated "cluster states" are actually this type of state as many $\mathcal{H}$-graph states are related to cluster states via local phase rotations. The $\mathcal{H}$-type state corresponds to the Gaussian state whose graphical structure is in the form [90]

$$\mathbf{Z} = i\,\exp(-2\alpha\mathbf{G}), \tag{53}$$

where α is a unitless parameter corresponding to squeezing strength. It can be shown that this type of state can be generated with generalized version of parametric downconversion [90]. This fact means that they can also be engineered by entangling various EPR states appropriately. The form of the $\mathcal{H}$-graph state is also useful as it can be generated in the frequency domain from a single optical parametric oscillator (OPO) by engineering the pump light and the Hamiltonian. We will discuss this in Sec. VI.

3. GHZ state

The N-qubit version of Greenberger-Horne-Zeilinger (GHZ) state is given by

$$|\psi\rangle = \frac{1}{\sqrt{2}}(|0\rangle^{\otimes N} + |1\rangle^{\otimes N}). \tag{54}$$

The GHZ state is known to be useful for various quantum tasks such as quantum communication and teleportation network. The continuous variable version is defined by the nullifiers given by [98]

$$\hat{\delta}_1 = \sum_i \hat{p}_i, \tag{55}$$

$$\hat{\delta}_j = \hat{x}_j - \hat{x}_{j+1}, \tag{56}$$

with $1 < j < N-1$. It can be shown that the $\mathcal{H}$-graph representation of the GHZ state is an all-connected graph with $\mathbf{G} = \mathbf{I} - \mathbf{J}$ where $\mathbf{J}$ is the matrix where all elements are 1 [90]. If we perform Fourier transformation on every single mode but one (which we will denote as mode 1) and take some linear combination, we have a new set of nullifiers as

$$\hat{\delta}'_1 = \hat{p}_1 - \sum_{k\neq 1} \hat{x}_k, \tag{57}$$

$$\hat{\delta}'_j = \hat{p}_j - \hat{x}_1, \tag{58}$$

with $2 < j < N$. The new nullifiers have the form of the cluster state whose graph is a star graph (Fig. 5). This here shows the equivalence between the all-connected $\mathcal{H}$ graph and the star graph represented with $\mathbf{Z}$.

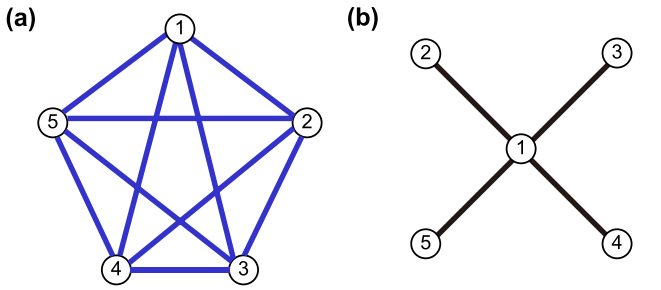

FIG. 5. Graphical representation of the GHZ state. As an example, we show the case with five modes. (a) $\mathcal{H}$-graph representation as all-connected graph. (b) Representation using $\mathbf{Z}$ after the Fourier transform of a single mode as a star graph.

VI. GENERATION OF OPTICAL CONTINUOUS-VARIABLE QUANTUM ENTANGLEMENT WITH MULTIPLEXING

So far we have discussed the general description of CV quantum entanglement. From this section, we will discuss how the optical system allows us to generate large-scale quantum entanglement.

In most of the generation of the small-scale entanglement, one squeezed-light source is used per one mode of the entanglement. This highly limited the scale of the entanglement. Moreover, as CV quantum entanglement is a phase-sensitive state, the more linear optics required in the systems, the more parameters that are needed to be controlled and stabilized. The idea of multiplexing for the generation of large-scale quantum entanglement is based on the fact that the optical system is rich in degrees of freedom such as polarization, time, frequency, and spatial mode. By multiplexing in these degrees of freedom, it is possible to make various modes interact using the same optical components. The fact that the optical system is a propagating wave system and not a static qubit also helps in this regard; light modes can pass through the optical components without staying there, allowing other light modes to enter the same component and repetitively interact. As a side

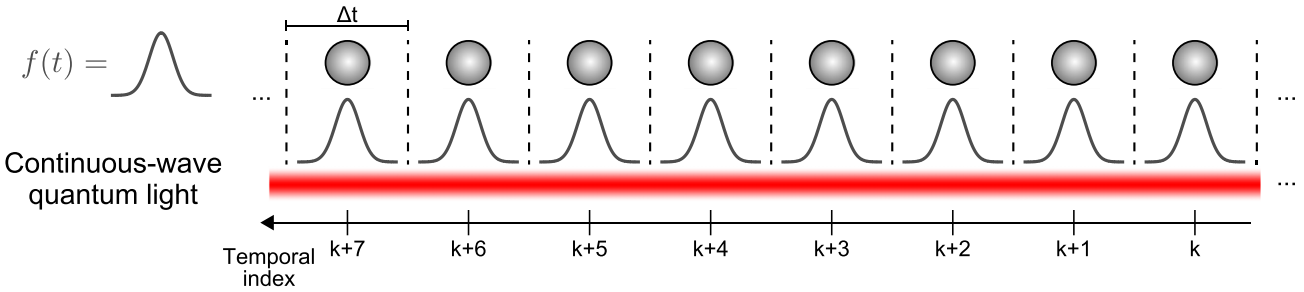

FIG. 6. Conceptual diagram of time-domain multiplexing. Here we assume that the quantum state of light is generated with continuous wave, which is usually the case in the actual experiments. The shape of the wave packet $f(t)$ is assumed to be the same in all time bins of temporal width Δt that are labeled by index k. This assumption is made so that the temporal mode can interact with each other. The circle nodes correspond to each wave-packet mode that is usually shown in the graphical representation.

note, we also see development of nonchip components which could further assist the large-scale entanglement by making the required components more compact [99,100].

In this section, we will look at the large-scale generation of quantum entanglement based on three popular multiplexings: time-domain multiplexing, frequency-domain multiplexing, and spatial-mode multiplexing.

A. Time-domain multiplexing

Figure 6 shows the concept of time-domain multiplexing. In time-domain multiplexing, we encode the information in a temporal wave packet and have the wave packets interact by using the optical delay line and linear optics [36]. If we let Δt be the time width of the wave packet and $f(t)$ be the shape of the wave packet which is assumed to be real, we can write the annihilation operator $\hat{a}_f$ associated with this mode as

$$\hat{a}_f = \int_{-\infty}^{\infty} dt\, f(t)\hat{a}(t), \tag{59}$$

where $\hat{a}(t)$ is an annihilation operator at time t which satisfies a commutation relation

$$[\hat{a}(t), \hat{a}^\dagger(t')] = \delta(t - t'). \tag{60}$$

Note that for the $f(t)$ here, we considered a rotation reference frame of the carrier frequency and all the following discussions hold for the wave packet $f(t)$ whose frequency spectral is localized near the carrier frequency, which is almost always the case for an optical system as the optical carrier is on the order of a few hundred terahertz. Moreover, we will ignore dispersion in this argument, meaning that the wave packet can be considered as only the function of time.

As we are multiplexing the temporal mode on a same spatial beam and want them to interact, we usually denote the temporal index as k and consider the temporal mode at that timing as $f_k(t) = f(t - k\Delta t)$ which is simply a translation of the original mode function. This is important as we would want them to interact with each other.

There are a few conditions, both theoretically and experimentally, that these wave packets should satisfy. First, we would want the mode to represent the bosonic mode. Therefore, if we look at the commutation relation, we have

$$\begin{aligned}[\hat{a}_{f_k}, \hat{a}^\dagger_{f_l}] &= \iint dt\, dt'\, [\hat{a}(t), \hat{a}^\dagger(t')] f_k(t) f_l^*(t') \\ &= \int dt\, f_k(t) f_l^*(t'). \end{aligned} \tag{61}$$

Thus, if we select $f(t)$ so that it is normalized and are orthogonal when it is shifted by Δt, the bosonic commutation relation can be satisfied.

Another important aspect is that we want to be able to measure the quadrature of each mode individually. For that, let us consider the quadrature operator for the wave-packet mode $f(t)$. Using the definition of quadrature, we can readily write the quadrature $\hat{x}_f$ as

$$\hat{x}_f = \sqrt{\frac{\hbar}{2}} \int dt\, [f(t)\hat{a}(t) + f^*(t)\hat{a}^\dagger(t)]. \tag{62}$$

For a mode function that is real, we have

$$\hat{x}_f = \int dt\, f(t)\hat{x}(t) \tag{63}$$

with

$$\hat{x}(t) = \sqrt{\frac{\hbar}{2}}[\hat{a}(t) + \hat{a}^\dagger(t)]. \tag{64}$$

Note that the above equation holds for other phases aside from the x quadrature as well. This means that we can just choose and measure the temporal signals at the phase of our interest and then postprocess by integrating with the shape of the wave packet $f(t)$ to retrieve the quadrature $\hat{x}_f$. This simplicity makes time-domain multiplexing a nice choice as each wave-packet mode can be easily accessed by changing the phase of the local oscillator (LO) at the timing required. For many tasks, we need to measure each mode $f_k(t)$ and $f_l(t)$ with different bases. Hence, it is important that the mode function we select is not only orthogonal, but also contained within the time-bin width Δt.

Strictly speaking, $\hat{x}(t)$ does not mathematically satisfy the criteria for the usual quadrature operator; the temporal signal measured from the homodyne does not correspond to this. However, if we are considering the $f(t)$ whose frequency bandwidth is sufficiently smaller than the detection bandwidth of the homodyne detector, we can use the homodyne detector signal as $\hat{x}(t)$ and Eq. (63) gives the correct quadrature for the

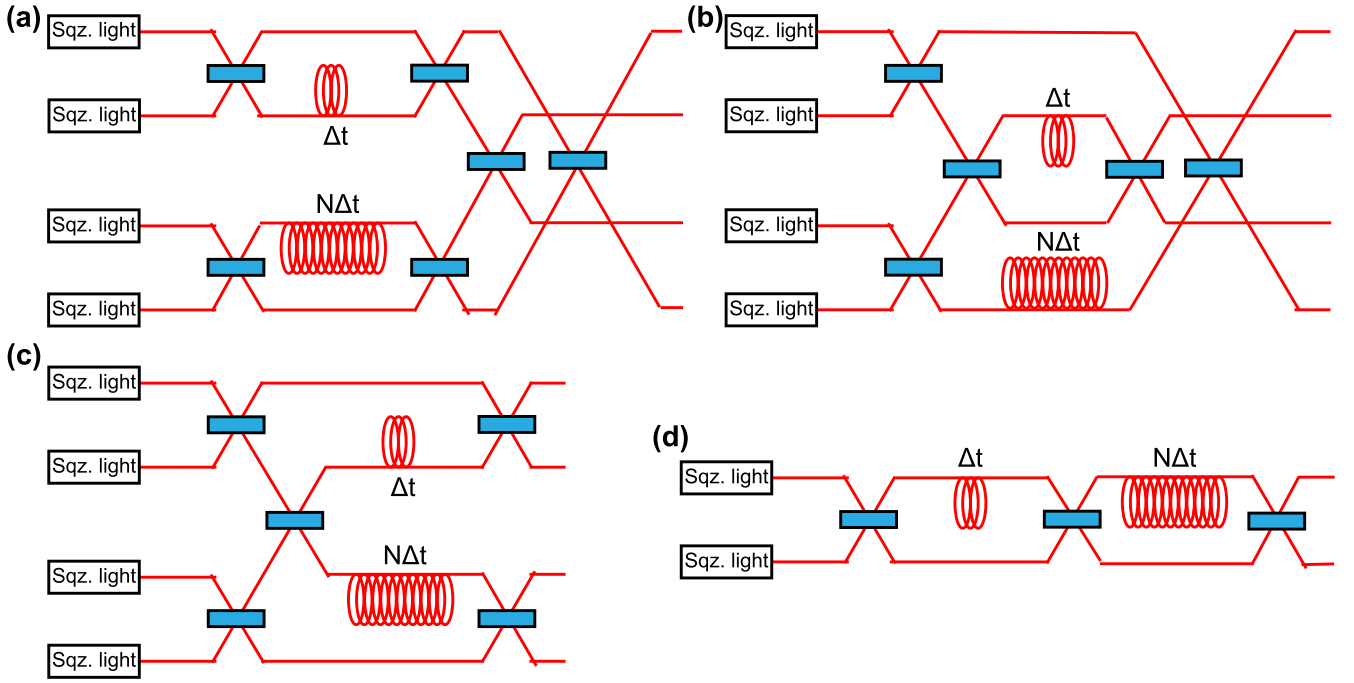

FIG. 7. Various setups for generation of time-domain-multiplexed cluster states. Sqz. light: squeezed light. (a), (b) Setups for quad-rail lattice [36] and bilayer square lattice [37], while (c) and (d) are the experimental setups in Refs. [53] and [54], respectively.

mode function we want. Another way of thinking about this is to actually measure $\hat{x}(t)$; we need the homodyne detector with infinite-frequency bandwidth, and the physical homodyne detector corresponds to sampling with finite-time resolution.

In the discussion so far, we have not discussed how to determine the wave-packet width Δt. In principle, we would want this Δt to be as small as possible so that we can pack the wave packets close to each other. This, however, is limited by the parameters of the systems. The first limitation is the frequency bandwidth of the squeezed-light source. When doing time-domain multiplexing, we want to consider each wave-packet mode as an independent squeezed state. If we calculate the correlation between the quadrature (for example, x quadrature) of two adjacent modes, we have

$$\langle \hat{x}_k \hat{x}_{k+1} \rangle = \frac{\hbar}{2} \iint dt\, dt' f_k(t) f_{k+1}(t') \times \langle [\hat{a}(t) + \hat{a}^\dagger(t)][\hat{a}(t') + \hat{a}^\dagger(t')] \rangle, \quad (65)$$

where the mean is taken with respect to the squeezed light generated from the source in the time axis. If the generated light has no temporal correlation, the above mean $\langle \dots \rangle$ is nonzero at only $t = t'$ and the orthogonality of the mode ensures that $\langle \hat{x}_k \hat{x}_{k+1} \rangle = 0$. In the actual squeezed-light source, however, there is always a finite temporal correlation. For instance, at the weak pump limit, the light from traditional optical parametric oscillator (OPO) has a temporal correlation of [101,102]

$$\langle \hat{a}(t) \hat{a}(t') \rangle \propto \exp(-\gamma |t - t'|), \quad (66)$$

where γ is the cavity decay constant of the OPO [102]. Therefore, even if the mode function is selected so that they are contained in the time bin Δt, the finite-frequency bandwidth of the light source could make the state of the squeezed light in the temporal mode inseparable. Note that this is the property of the squeezed-light source. Therefore, the frequency bandwidth of the squeezed-light source limits how small we can select Δt while preserving the independence between the temporal modes.

The frequency bandwidth of the squeezed-light source also limits the amount of the squeezing level we can get when we make the entangled states. If we suppose that the frequency spectral of the squeezing from the light source is given by $\tilde{S}(\omega)$ where ω is the angular frequency, then the amount of the squeezing S_f in mode $f(t)$ is given by [102]

$$S_f = \int d\omega |\tilde{f}(\omega)|^2 \tilde{S}(\omega), \quad (67)$$

where $\tilde{f}(\omega)$ is the Fourier transform of the mode $f(t)$. Thus, when the frequency bandwidth of $\tilde{S}(\omega)$ is limited, the squeezing level S_f will degrade if we make the mode $f(t)$ too narrow [$\tilde{f}(\omega)$ becomes broad]. Taken the above consideration, we can define our time-bin width Δt and the shape of the wave packet $f(t)$. After that, the temporal-mode squeezed state can be made to interact. Figure 7 shows the various experimental setup for the generation of time-domain-multiplexed quantum entanglement. Despite the differences in the setup, the key component that makes the temporal modes interact and weaves them into a large-scale entanglement is the optical delay line. As we want the time bins to correctly interact with each other, the long optical delay line has to be an integer time of Δt. Figure 8 shows the structures of the two-dimensional cluster states that have been experimentally realized [53,54]. As both of the dimensions are time, we can see the spiral structure of the entanglement. The more the number of the

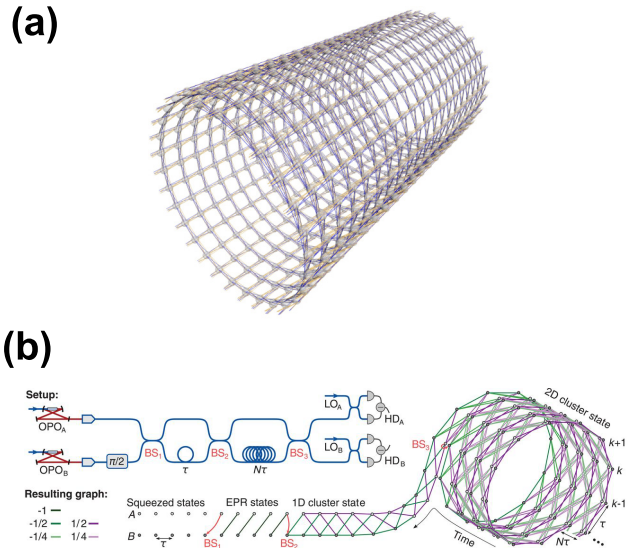

FIG. 8. Graphical representation of time-domain-multiplexed cluster state generated in [53] (a) and [54] (b) (reproduced from [53] and [54] with permission).

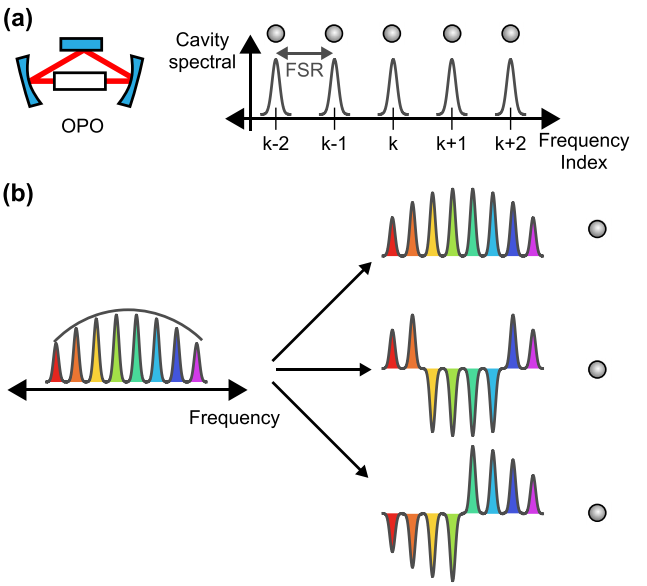

FIG. 9. Conceptual diagram of frequency multiplexing. (a) Multiple resonant frequency mode from an optical parametric oscillator (OPO). Each peak is separated in the frequency by a free-spectral range (FSR). If the separation is large compared to the linewidth, each cavity peak can be considered as an independent bosonic mode. (b) Supermode, which is a linear combination of binned frequency mode within the phase-matching region of the nonlinear medium.

optical delay lines allow a more complicated structure of the entanglement. The length of the delay line will eventually be limited by practicability and coherence time of the master laser. For the case where only static components are used, the entanglement generated from this method will have periodicity as the lights enter and come out of the same optical components. This is also the case for various demonstrations of cluster state generation experiments [51–54]. On the other hand, if we add dynamic components such as a variable beam splitter, it is possible to tailor various entanglement structure [96].

Measuring the time-domain-multiplexed quantum entanglement is also straightforward. The modes here are the temporal wave packets of the propagating light which can sequentially enter the homodyne detectors and are individually measured. Thus, accessing and manipulating each mode of the entanglement can be done relatively easy, and the number of the homodyne detectors required is equal to only the number of the spatial beams used. Verification of the entanglement using vLF criteria in Sec. V C is also relatively straightforward as each mode is measured individually.

B. Frequency-domain multiplexing

Frequency-domain multiplexing can be considered complementary to time-domain multiplexing as time and frequency are related via Fourier transformation. In the frequency-domain multiplexing, the modes are taken to be each frequency comb. The characteristic of this method is that the frequency comb can be generated in a single time step. Frequency domain is also one of the main approaches to multiplexing and there are various theoretical [38,40,44,45,50] and experimental [57–62,64–68] researches in this direction. There are also proposals where time-domain and frequency-domain multiplexing are combined [38,103,104].

Figure 9 shows two approaches in defining the frequency mode of the frequency-domain multiplexing. If we are using OPO, we can define each resonant frequency mode of the cavity as the mode for our entanglement and the quantum entanglement is multiplexed using the cavity mode [Fig. 9(a)]. We can also define supermodes [50] which are the orthonormal set of the modes defined by their frequency spectrum, and consider the entanglement between them [Fig. 9(b)]. In this approach, rather than individual frequency comb or resonant frequency mode, the mode is taken as a linear combination of binned frequency comb. Below we show two examples that illustrate the basics of two approaches.

Figure 10(a) shows the schematic of the generation diagram for frequency-domain-multiplexed entanglement based on cavity resonant modes [57]. The basic ideas are similar to the time-domain-multiplexing method; from a single (or a few) squeezed-light source, we generate squeezed states or small entangled states that are multiplexed in frequency. Then, these modes can be put through optical components such as beam splitters which can act on all the frequency modes and connect them into a large-scale quantum entangled states.

To be more explicit, the OPO is pumped using two different frequencies at two different polarizations. This creates two-mode squeezed states in frequency modes in both polarizations. The frequency modes that are entangled, however, are also different because the pump is in a different frequency. After that, the two-mode squeezed states in the frequency modes in both polarizations interact using a polarization beam splitter and a half-wave plate which acts as beam-splitter interaction between two polarization modes. This beam-splitter interaction acts on all frequency modes allowing the generation of a large-scale entanglement. The fact that many optical components are nonselective with respect to a certain mode

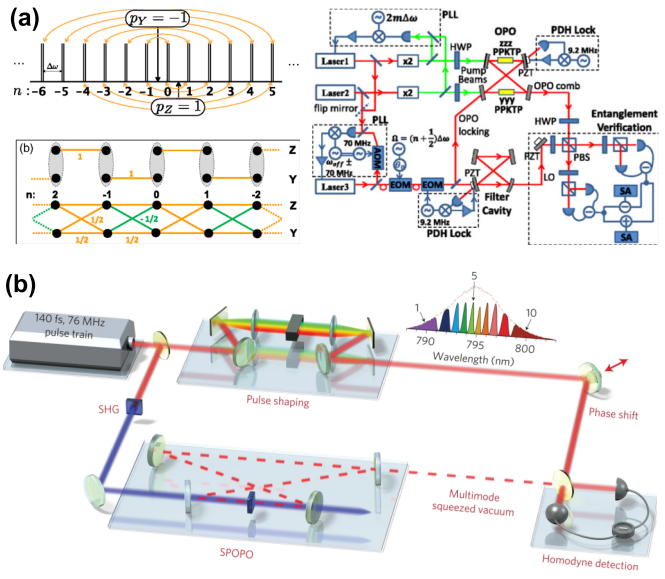

FIG. 10. Experimental setup for generation of quantum entanglement multiplexed in frequency domain. (a) Generation using resonant peaks of cavity [57]. (b) Generation of frequency-multiplexed entanglement in supermode (reproduced from [60] with permission).

(in this case frequency) makes multiplexing possible. The resulting entanglement in this case is a dual-rail structure [36].

Figure 10(b) shows the experimental setup for the generation of the entanglement in frequency domain based on the super mode [60]. Similar to the former approach, the entanglement can be engineered by the pump light of the OPO and the measurement is done using LO whose frequency profile has been tailored. For the former approach, the mode separation is determined by the free-spectral range of the OPO, while the frequency spectral of modes here are not separated as the frequency combs are binned into the frequency bin and the linear combinations are taken so that the modes are orthogonal.

The main limitation of the frequency-domain multiplexing is the phase-matching bandwidth of the nonlinear medium of the squeezed-light source. When the OPO is pumped, the number of frequency modes generated is limited by the phase-matching bandwidth. As the frequency mode approaches the cutoff frequency of the phase matching, the squeezing level becomes smaller until there is no squeezing present at all. In the case where OPO is used, the number of the frequency mode that can be generated at once is roughly the phase-matching bandwidth divided by the free-spectral range of the OPO. As an example, in Ref. [57], they estimated the number of generated modes to be about 6000 modes, where the number of modes actually measured is 60 modes, limited only by the technology level in that time. For the case of the entanglement in the supermode, the number of modes depends on the frequency resolution that one can tailor the pump and the LO of the local oscillator. This is also limited by the phase-matching bandwidth, as broader phase-matching bandwidth mean that it is easier to bin the frequency.

Regarding the measurement of the frequency-domain-multiplexed quantum entanglement, if we want to measure the quadrature of each mode, as all the modes are generated and arrive at the same time, we have to demultiplex the frequency mode (for example, by using grating) to be able to implement homodyne measurement of each frequency mode. For the case where the linear combination of the quadrature is what we want to measure, this can be done by using frequency combs with appropriate relative phases between each comb as an LO and lock the relative phase between each comb. This was in fact implemented experimentally in the generation of the frequency-domain-multiplexed cluster state [57,68]. For the supermode case, a similar approach can be taken to measure multiple supermodes simultaneously.

C. Spatial-mode multiplexing

Another method of multiplexing that has been researched is the multiplexing in the spatial mode [69–74]. There are methods that use a specifically designed OPO system that allows generation of entanglement between different spatial modes [69–71,73] or atomic systems which generate entanglement in optical orbital angular momentum [72,74]. Atomic systems have high affinity with this approach as optical orbital angular momentum can couple with atomic spin. There is also a proposal for generation of quantum entanglement where both spatial mode and temporal mode are used in multiplexing [105].

To do the measurement on the individual mode, the generated entanglement must be demultiplexed. Although there are researches on spatial-mode demultiplexing [106–108], the technology still remains challenging and many of the verifications of the spatial-mode entanglement are not done with mode demultiplexing. Figure 11 shows an example of the experimental setup in the generation of spatial-mode-multiplexed cluster state [47]. In this setup, the OPO is designed so that when it is pumped, instead of typical Hermite-Gaussian modes, the Laguerre-Gaussian modes are generated and they are entangled. The phase-matching condition for the Laguerre-Gaussian mode is analogous to the conservation of angular momentum [46]. By pumping the OPO with pump light with different angular momentum, a similar approach taken in the frequency multiplexing can be done which results in the entangled state. Thus, one can think of this type of entanglement generation as a spatial-mode comb. The nonlinearity of the nonlinear medium, however, is dependent on the shape of the spatial mode which could result in a different level of correlation across the state. This eventually limits the number of the modes that can be generated using this methodology.

VII. EXPERIMENTAL TOOLBOX FOR OPTICAL CV QUANTUM ENTANGLEMENT

In this section, we will discuss various experimental elements for the large-scale generation of the CV quantum entanglement. As we have seen, there are three basic components: squeezed-light sources, linear optics (i.e., beam splitter), and homodyne detector.

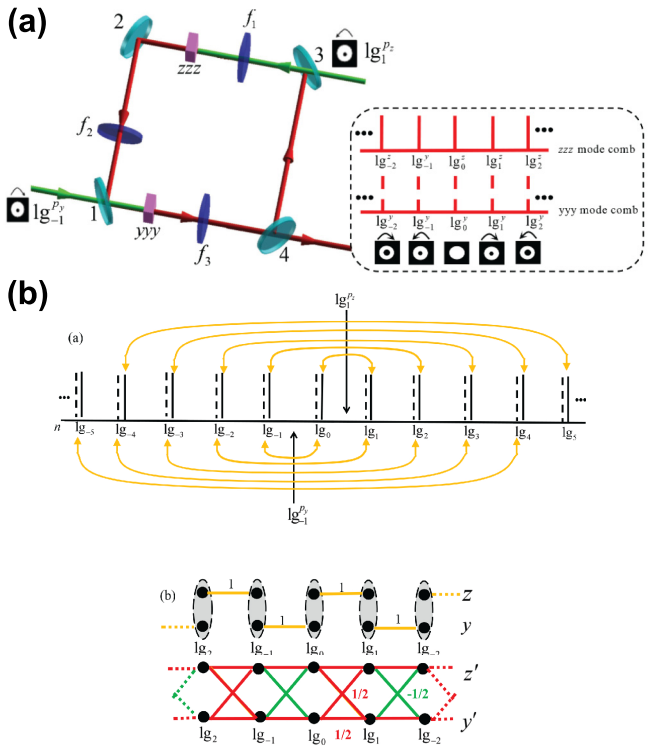

FIG. 11. An example of the setup for the spatial-mode-multiplexed quantum entanglement generation. (a) Setup for generation of quantum entanglement in Laguerre-Gaussian modes. (b) The resulting entanglement in spatial-mode comb. Adapted with permission from [47].

A. Squeezed-light sources

Squeezed light is an important resource not only in the generation of optical quantum entanglement, but also for quantum optics in general. Generation of squeezed light has a long history beginning from the generation using third-order optical nonlinearity [19] in 1985 and second-order optical nonlinearity [18] in 1986. After that, although the technological components have seen much development over many years, the basic concepts have not changed.

For the bulk optics systems, generation of the squeezed light is usually based on the second-order optical nonlinearity. The basic configuration is based on a nonlinear crystal structure which is called optical parametric amplifier (OPA). For the generation of squeezed light in the continuous-wave (CW) system, sometimes cavity structure is also added to amplify the nonlinearity and such structure is called optical parametric oscillator (OPO). Generation of squeezed light in both OPA and OPO has been widely researched and we outline a few notable results below. The readers should consult a more specific review for more details [21]. The current record of the squeezing level in CW system is 15 dB of squeezing at 1064 nm [109], and 12.3 dB [110] and 12.6 dB [111] of squeezing at 1550 nm. The bandwidth of the squeezed light of both experiments is on the order of tens of megahertz. On the other hand, for the pulsed laser, the record is about 5.8 dB of squeezing [112,113]. Frequency bandwidth of the squeezed light is also an important parameter for multiplexing. In the CW system, we have a bulk OPO with about 65-MHz bandwidth with 8 dB of squeezing [114], and a system with 1.2-GHz bandwidth and 3 dB of squeezing [115]. For the waveguide-based system, the OPA-based squeezed-light source has shown to have about 6-THz bandwidth with 6.3 dB of squeezing using optical spectrum analyzer measurement [116]. The direct quadrature measurement using homodyne detector has observed 5 dB of squeezing with 43-GHz bandwidth [117] and 8 dB of squeezing with 200-MHz bandwidth [118]. For the pulsed-light system, the bandwidth translated to repetition rate and has currently reached 156 MHz in the squeezed state experiment [65]. Although integrated photonics and silicon photonics offer a smaller and integrated system, the current squeezing level in such system is still very low. For instance, the squeezed-light measurement with nanophotonics homodyne measurement observing about 1.0 dB for 9-GHz bandwidth [119], and generation and measurement of 1.0 dB squeezed light with 1-GHz bandwidth generated and characterized on chip with silicon nitride microring resonator [120] have been recently reported.

Depending on the tasks, the required squeezing level of the squeezed light to make an entangled state is different. If we consider our task to be quantum computation with fault tolerance, then it is expected that quantum entangled states whose nullifiers have squeezing level of around 10 to 15 dB is required [121]. For the tasks that only used the correlations such as quantum computation, only the squeezing level matters as the contributions due to antisqueezing are usually erased via measurement and feed forward [122]. For some tasks such as state engineering, this is usually not the case. In that regard, bulk-type or OPA-based squeezed-light source is currently deemed more reachable. Although spatial integration might still be needed, multiplexing technique could be used to reduce to level of integration required or we can also just used bulk optics for generation of large-scale entanglement of certain structure where the number of the squeezed-light sources is not high.

B. Linear optics

Linear optics components are very well established. For the bulk optics, the losses in mirror, lenses, and beam splitter can be made negligible with good coating. For integrated optics, the optical losses are still relatively high. For the generation of large-scale quantum entanglement with multiplexing method, requiring only a few optical components helps reduce the effects of the optical losses. The difficulties in the linear optics for the entanglement generation come from the requirement of the phase locking and interferometric visibility. As squeezed lights are phase-sensitive states, we have to do the phase locking between them whenever they interfere. The phase noise degrades the squeezing level, thus the quality of the entanglement. When two lights are interfered, their modes (spatial, temporal, spectral, and polarization) must also be matched so that they can interfere. In both regards, integrated photonics are more convenient than bulk optics as lights are confined in a well-defined mode making mode matching high and phase control can be done even with passive control. Multiplexing technique also makes phase control and mode matching easier as the number of the physical components that needed to be controlled and adjusted are much lower than the

same entangled states generated without any multiplexing. In our opinion, the number of the classical parameters required to stabilize the system will be the practical limitation of how large the quantum system can be.

Optical delay line also plays an important role. The most common platform for the delay line is an optical fiber. Although there are researches on on-chip optical delay line [123] and free-space-type delay line using mirrors is quite common in proof-of-principle experiments, the length requirement and its simplicity make optical fiber the leading candidate. The imperfections in the delay line come from the propagation loss and coupling loss. The propagation loss is dependent on the wavelength, and if we use C band, the propagation loss can be as low as 0.3 dB/km @ 1550 nm [124]. On the other hand, the coupling loss comes from the fact that we have to couple the free-space light or the on-chip system to the fiber, and direct coupling between them can have some mode mismatch. For the free-space system, with proper alignment, the mode matching can go up very high as 96% [51], while for the integrated system, there are researches on efficiently coupling light between fiber and on-chip components using tapered fiber and evanescent wave [125].

C. Homodyne detector

After the large-scale quantum entanglement is generated, it is crucial that it is measured. For the CV system, the main measurement on the entangled state is the homodyne measurement. The main parameters of concern for the homodyne detector are efficiency, clearance, and bandwidth. The quantum efficiency of the homodyne detector directly corresponds to the loss and is mainly determined by the photodiodes. Silicon photodiode for near infrared and InGaAs photodiode for C band with quantum efficiency of above 99% are available [109]. The quantum efficiency, however, has a tradeoff relation with the bandwidth of the detector. The bandwidth of the homodyne detector determines how small we can multiplex the information in the time domain or how fast can the repetition rate be in the frequency domain. This is limited mainly by the capacitance of the photodiode. To have high efficiency, the photodiode must have certain thickness which increases the capacitance and limits the bandwidth. This effect has been theoretically explored [126]. In addition to these two parameters, the electrical part of the circuit also plays an important role. The power of the optical local oscillator put into the homodyne detector must be sufficient so that the shot-noise level is well above the circuit-noise level. This clearance limits the detection noise of the homodyne detector. Although it should be possible to put as much local oscillator power, it is limited by the saturation power of the photodiode.

Although the homodyne detector is an established technique, the frequency bandwidth of high-efficiency homodyne detectors used in quantum experiments is currently limited to about a few hundred megahertz. Recently, by using OPA as an optical preamplifier, this bandwidth has been greatly improved [117,127,128] and we have seen measurement of squeezed light on the gigahertz order with lossy homodyne detectors. Preamplification with OPA opens the possibility of measuring nonclassical light and quantum entanglement with broadband homodyne detectors that are commonly used in the telecommunication. It is important that the amplification via OPA acts equally on all the multiplexed modes, i.e., the amplification gain does not differ between modes. The gain flatness and the frequency bandwidth of OPA will play an important role for the detection of large-scale quantum entanglement generated with the multiplexing method.

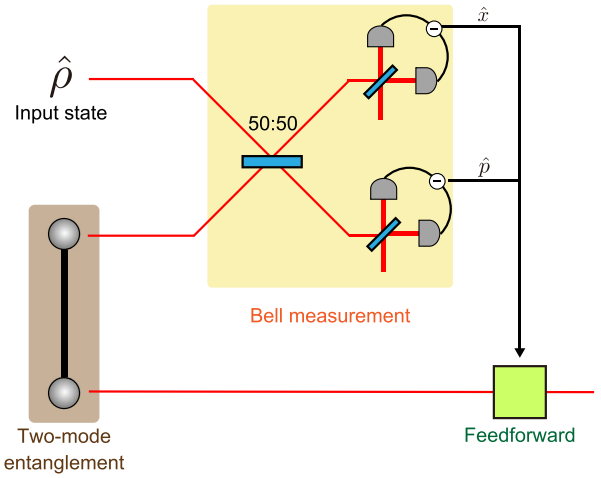

FIG. 12. Conceptual diagram of quantum teleportation.

VIII. APPLICATIONS OF LARGE-SCALE OPTICAL QUANTUM ENTANGLEMENT

In this section, we will discuss various applications for the large-scale quantum entanglement. As the subjects are very broad, we do not claim to have thoroughly covered every subject. We will give our main focus to the applications of the large-scale cluster-state-type entanglement whose large-scale generation has been widely demonstrated.

A. Quantum teleportation

The most basic application of quantum entanglement is quantum teleportation [129–131]. Quantum teleportation was first demonstrated in optical systems for both the DV system [15] and CV system [22]. Figure 12 shows the basic idea of quantum teleportation. In quantum teleportation protocol, a state to be teleported is mixed with one mode of the quantum entanglement and the two modes are jointly measured using the Bell measurement. By feed forwarding the measurement results to another mode of the entanglement and performing operation on it depending on the measurement results, the input state is teleported to the output mode.

The key to quantum teleportation relies on the fact that although the measurements at each mode of the quantum state give random values, they are correlated in a nonclassical way. The feed-forward operation removes the randomness of the measurement results using the fact that we know the form of the quantum entanglement. In CV teleportation, the ideal resource is an EPR state with the correlation, i.e., the nullifier, of $\hat{x}_1 - \hat{x}_2 = 0$ and $\hat{p}_1 + \hat{p}_2 = 0$. In reality, the nullifiers will not be perfectly zero and it can be shown that the variances of these two nullifiers directly determine the amount of the

noises that are added to the quadrature of the teleported state [97].

B. Measurement-based quantum computation

Although the quantum teleportation protocol can be viewed simply as an identity operation where the input and output states are the same, the essence of quantum teleportation protocol is important in quantum computation using large-scale quantum entanglement. In 2001, Briegel and Raussendorf proposed a quantum computing method called one-way quantum computation or measurement-based quantum computation (MBQC) [95]. In this approach, a large-scale quantum entanglement called *cluster state* is first generated, and each mode of the cluster state is then measured according to the desired quantum operation. In 2006, Menicucci *et al.* extend the idea of MBQC to the CV system [81]. One way to think about MBQC is that if we have an entangled state with appropriate structure, by measuring some of the modes, we can tailor the entanglement into any type of correlation corresponding to quantum operation we want. During such measurement, however, the classical values obtained will have some randomness which can be eliminated via feed-forward operation similar to the quantum teleportation protocol.

MBQC is a powerful approach in a sense that once we have generated the cluster state, we only have to do local measurement and feed-forward operation to implement quantum computation. This makes MBQC an appealing candidate for optical quantum computation as generation of large-scale quantum entanglement can be done via multiplexing. In fact, there have been various demonstrations of cluster states with various entanglement structure in the time domain [51–54], frequency domain [57,59,66], and spatial mode [71]. A feature of the generated cluster states is that their graph structures are periodic, making it highly compatible with multiplexing.

For the cluster state to be useful in MBQC, not only must they have large scale, but we must be able to access each mode individually as the individual measurement on each mode determines our computation. This is trivial for the CV cluster state without multiplexing and has been experimentally demonstrated [23,24,26,29]. For the multiplexed large-scale cluster state, implementations of Gaussian operations via local homodyne measurement on each wave-packet mode have been demonstrated for the time-domain-multiplexed cluster state [55,56] (Fig. 13). In this case, as the modes are temporal wave packets, they enter the homodyne detector sequentially, and we do not need extra demultiplexing. We only need to modulate the phase of the LO, which can be very fast even up to tens of gigahertz with the commercially available modulator.

The CV cluster state and homodyne measurement are not sufficient for universal quantum computation and some sort of non-Gaussianity is needed. We will discuss this in Sec. IX.

C. Quantum error correction

Another important application of quantum entanglement is quantum error correction. When we encode the quantum information, we need redundancy to mitigate the effect of errors and make the quantum information resilient. In the CV system, the current promising approach is that we encode a qubit such as Gottesman-Kitaev-Preskill qubit [132] in the CV system, and then encode them into a higher-level code [133,134] which relies on quantum entanglement.

To do quantum error correction, the type of entanglement we need is no longer a multimode Gaussian state, but a complicated non-Gaussian type of entanglement as the qubit needs to be a non-Gaussian state. Engineering such non-Gaussian entanglement is in general difficult as non-Gaussian generation is probabilistic in optical systems. There are, however, many proposals to overcome these difficulties. One of the approaches is that we can use the Gaussian toolbox to generate a type of entanglement called three-dimensional cluster state or Raussendorf-Harrington-Goyal (RHG) lattice and then replace each mode with the GKP qubit [41,49,133–135]. If we have sufficient GKP-qubit sources, it is also possible to proceed to generation of RHG lattice with GKP qubit directly [136,137]. The RHG lattice is a basic unit for surface code which is known to have relatively low threshold at a cost of requiring a large number of physical qubits per logical qubit. The replacement of mode with GKP qubit can be done either during generation process [49] or they can be teleported if the state is made with such structure. Experimentally, although non-Gaussian states are not added, there have been demonstrations of CV quantum entanglement of structure related to quantum error correction [68].

As a large number of modes are required in generation of the entanglement for quantum error correction, it is crucial to consider the quantum entanglement whose structure is compatible with multiplexing.

D. Quantum communication

Aside from the task in quantum computation, quantum entanglement is also useful in the communication tasks. The term quantum communication could refer to sharing quantum information between multiple parties such as quantum network or quantum internet [138], or transmission of information with quantum system, such as quantum key distribution and cryptography [139].

Regardless of what physical system will eventually be used for quantum computation, the optical system will be required for the communication tasks as it is currently the only propagating wave system that can carry quantum information over the distance. If we want to share the quantum state between multiple parties, one possible way to do it is to share GHZ-type entanglement between all the parties. By having some party measure their modes in a certain basis, an EPR pair can be induced between any two parties [140]. A proof-of-principle demonstration of this kind of quantum teleportation network has been already demonstrated in the optical system [33]. Quantum secret sharing protocol [141–144] also utilizes quantum entanglement. Optical quantum entanglement can also be useful for anonymously broadcasting classical information [145]

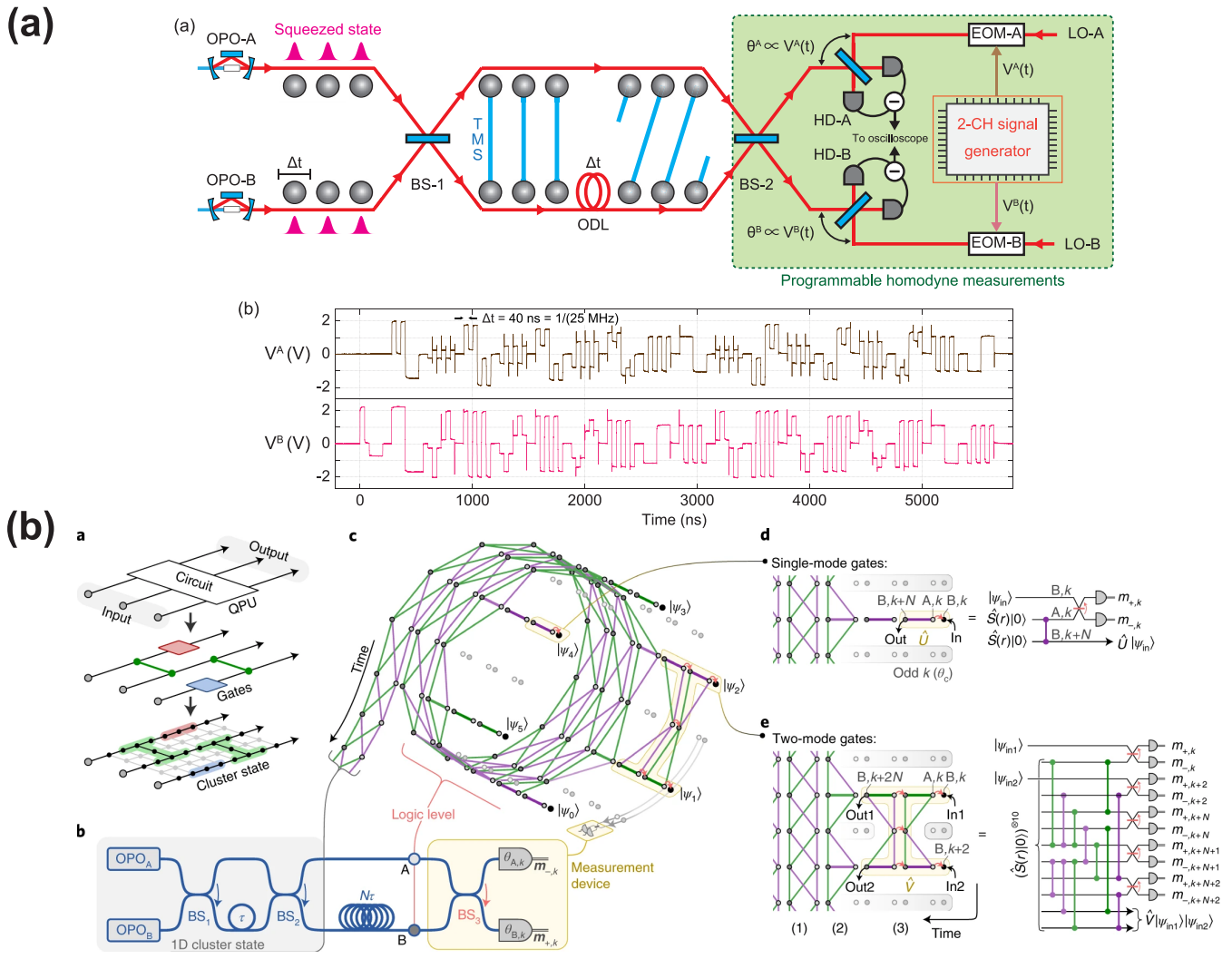

FIG. 13. Demonstration of measurement-based Gaussian operations using time-domain-multiplexed cluster state. (a), (b) From Refs. [55] and [56], respectively [(b) is reproduced from [56] with permission]. In both experiments, Gaussian operations are implemented via sequential CV teleportation in the time domain where the phase of the local oscillators is programmed according to the desired operations.

IX. FUTURE PERSPECTIVE

In this section, we discuss the future perspective of large-scale quantum entanglement. Here we will focus on two aspects. The first aspect is combination of large-scale quantum entanglement with non-Gaussian elements. This direction is required if we want to make the generated large-scale quantum entanglement capable of various applications mentioned in Sec. VIII. Many aspects of non-Gaussian quantum optics is so different from Gaussian quantum optics, and many efforts, both theoretical and experimental, are being made to describe and incorporate non-Gaussian elements to large-scale quantum entanglement.

The second aspect is how to increase the quality of the large-scale quantum entanglement. In Sec. VI, we have described the main multiplexing approaches via time, frequency, and spatial modes. Although each approach has its own advantages and disadvantages, all multiplexing methods allow efficient usage of optical components. Therefore, increasing the technological capability of each component, as we have discussed in Sec. VII, directly increases the quality of the large-scale entanglement, as the integration and scaling of the physical size of each component is no longer the main limitation. However, even with multiplexing, we still require a large number of modes for many applications such as quantum error correction. This can be achieved by combining various multiplexing methods. The bandwidth of each component also plays a crucial role as they allow much higher and denser multiplexing of optical modes and we will discuss this below.

A. Combining non-Gaussianity with optical quantum entanglement

In the optical system, the Gaussian toolbox is extremely powerful: generation of the squeezed state is an established technique, implementation of linear optics and beam-splitter interactions are straightforward, and all Gaussian operations can already be implemented. As we have seen from Sec. VIII,

the tasks that can be done with the Gaussian toolbox, however, are quite limited. For instance, for MBQC to be universal, we have to add non-Gaussian measurement or non-Gaussian state to the system [17,37,81,146], and for tasks such as quantum neural network [147] or quantum machine learning [148], non-Gaussian operations are used to generate the required nonlinearity. Thus, the next step in the research for large-scale quantum entanglement is how to add non-Gaussianity to them while retaining the scalability of the system.

There are already many different approaches toward this direction. Photon subtraction is the most primitive way to realize non-Gaussianity in CV optical system [149]. There are researches where mode-selective photon subtraction is done in the frequency-multiplexed entanglement [59,150]. Regarding this direction of development, there is also theoretical analysis on how photon subtraction affects the entanglement structure and theoretical properties of these types of non-Gaussian entanglements [151–156]. In the time domain, there is an experimental demonstration of time-gated photon subtraction [157], which could be useful for adding non-Gaussianity to a particular temporal mode of time-domain-multiplexed quantum entanglement.

An approach complementary to direct enacting of non-Gaussianity on to the entanglement would be to substitute some of the nodes of the entangled state in the graphical representation with a non-Gaussian state. As an example, it has been shown that probabilistic substitution of a node of a cluster state with a non-Gaussian state can be useful for quantum computation and quantum error correction, given that the substitution rate is above a certain threshold [49,135]. In this approach, as the direct substitution is implemented, an optical switch is a crucial component for switching between the Gaussian state and the non-Gaussian state.

For such purpose, the optical switch has to have low-loss, high-repetition rate, and fast-switching time. These properties, however, can be difficult to simultaneously realize. Free-space optical switching is usually based on Pockel cell which can have low loss, but usually has limited repetition rate due to its size. On the other hand, the fast switching based on silicon photonics can have a very high speed, but the loss is still high. There is also a proposal where instead of using the optical switch, the Gaussian entanglement is made with additional modes that can be used to substitute the mode with the non-Gaussian state via quantum teleport [158]. This method benefits from the fact that the switching is now done by changing the basis of the homodyne measurement which can be done with modulation of classical light. The additional modes, however, add more noises from the finite squeezing.

For MBQC, it is also possible to add the non-Gaussianity via the measurement using ancillary state and nonlinear feed forward [37,53,159]. When this is done, it allows the cluster state to be used for universal quantum computation. The high-speed system for such nonlinear feed forward has been recently demonstrated [160]. We could also consider replacing the homodyne detectors with the photon-number-resolving detector (PNRD) which would result in a task called Gaussian boson sampling (GBS) [161]. GBS is known to be a task that cannot be efficiently simulated on classical computer and can also be used for state engineering [162–164].

In the near future when non-Gaussian elements are added to the large-scale quantum entanglement, the experimental evaluations of such state will also be crucial. In the evaluation of large-scale quantum entanglement, the common underlying assumption is that the states are Gaussian. This assumption greatly simplifies the number of parameters that needed to be measured. For instance, for N-mode Gaussian entangled state, measuring N nullifiers could suffice for evaluation of many states, and even if we have to measure the whole covariance matrix, they only have $(2N)^2$ parameters. Comparing this to quantum tomography up to n-photon component, then we have the parameters on the order of n^{2N}. Although there is recent research for the non-Gaussian entanglement witness [165], we expect that development of the verification technique for large-scale non-Gaussian quantum entanglement will become a pressing task as the technology matures and engineering of complex non-Gaussian entangled state becomes more common.

B. Toward high-quality optical quantum entanglement

In the final section of this paper, we would like to reiterate the important points of optical quantum entanglement and what is required to make high-quality optical entanglement for quantum tasks.

Quantum entanglement comes naturally in the CV system. This is because Gaussian resources and operations can be efficiently implemented in the optical system, allowing for deterministic generation of entanglement. The optical system is also rich in degrees of freedom, making multiplexing and large-scale generation of quantum entanglement possible. Multiplexing is a common technique in telecommunication and the ability to combine this to the quantum system is the uniqueness of the optical system. The multiplexing techniques make integration and scaling down the physical sizes of individual components no longer a main limitation in scaling up of the size of entanglement as the required number of components does not scale with the size of entanglement anymore.

Although multiplexing has helped in lowering most of the hurdles regarding scalability, it has not removed all the hurdles. As it is expected that many physical qubits will be required for tasks such as quantum error correction and quantum computation, combination of multiplexing in time, frequency, and integration of optical components, rather than multiplexing of single degree of freedom, will be important to achieve the required scale for any applications. With this in mind, the development of the entanglement using each multiplexing method and integrated system should progress in a way that they are able to incorporate the strategy deployed in different multiplexing. For the time and frequency domains, this is rather straightforward as they are related by Fourier transform and there are already proposals that combined two types of multiplexing [38,40,103,104].

From a technological perspective, as we have discussed in Sec. VII, the bandwidth of each optical component determines the level of multiplexing we can achieve. This is similar to optical telecommunication technology where information can

be transmitted faster when a larger bandwidth is used. In time-domain multiplexing, bandwidth of both squeezed-light sources and homodyne detectors determined the size of the temporal wave packet, thus, how packed we can encode the optical mode. For frequency-domain multiplexing, the frequency bandwidth determined the number of the frequency modes we can utilize in the generation of the quantum entanglement. In the spatial-mode multiplexing, as the higher-order spatial modes have higher-frequency component, the broader the bandwidth of the squeezed-light source is, the easier it is to generate and access the quantum entanglement in higher-order mode. As the optical telecommunication technology is also headed toward broader and broader bandwidth, combining and importing components and techniques of telecommunication community will allow for the generation of better quality and even larger scale of optical quantum entanglement. Therefore, the next breakthrough in the large-scale optical quantum entanglement will be the hybridization between quantum optics and optical telecommunication. This will lead to the generation of even larger and more complex quantum entangled state than the impressive results we have reviewed in this paper.

ACKNOWLEDGMENTS

This work was partly supported by Japan Science and Technology (JST) Agency (Moonshot R&D) Grant No. JPMJMS2064, the UTokyo Foundation, and donations from Nichia Corporation. W.A. acknowledges the funding from Japan Society for the Promotion of Science (JSPS) KAKENHI (No. 23K13040) and support from the Research Foundation for Opto-Science and Technology.

[1] R. P. Feynman, Simulating physics with computers, Int. J. Theor. Phys. **21**, 467 (1982).

[2] M. A. Nielsen and I. L. Chuang, *Quantum Computation and Quantum Information* (Cambridge University Press, Cambridge, 2000).

[3] C. H. Bennett and G. Brassard, Quantum cryptography: Public key distribution and coin tossing, Theor. Comput. Sci. **560**, 7 (2014), theoretical Aspects of Quantum Cryptography – celebrating 30 years of BB84.

[4] S.-H. Wei, B. Jing, X.-Y. Zhang, J.-Y. Liao, C.-Z. Yuan, B.-Y. Fan, C. Lyu, D.-L. Zhou, Y. Wang, G.-W. Deng, H.-Z. Song, D. Oblak, G.-C. Guo, and Q. Zhou, Towards real-world quantum networks: A review, Laser Photonics Rev. **16**, 2100219 (2022).

[5] S. Pirandola, U. L. Andersen, L. Banchi, M. Berta, D. Bunandar, R. Colbeck, D. Englund, T. Gehring, C. Lupo, C. Ottaviani, J. L. Pereira, M. Razavi, J. S. Shaari, M. Tomamichel, V. C. Usenko, G. Vallone, P. Villoresi, and P. Wallden, Advances in quantum cryptography, Adv. Opt. Photon. **12**, 1012 (2020).

[6] S. McArdle, S. Endo, A. Aspuru-Guzik, S. C. Benjamin, and X. Yuan, Quantum computational chemistry, Rev. Mod. Phys. **92**, 015003 (2020).

[7] L. Bassman, M. Urbanek, M. Metcalf, J. Carter, A. F. Kemper, and W. A. de Jong, Simulating quantum materials with digital quantum computers, Quantum Sci. Technol. **6**, 043002 (2021).

[8] J. S. Bell, On the einstein podolsky rosen paradox, Phys. Phys. Fiz. **1**, 195 (1964).

[9] A. Aspect, P. Grangier, and G. Roger, Experimental realization of Einstein-Podolsky-Rosen-Bohm gedankenexperiment: A new violation of bell's inequalities, Phys. Rev. Lett. **49**, 91 (1982).

[10] R. Uola, A. C. S. Costa, H. C. Nguyen, and O. Gühne, Quantum steering, Rev. Mod. Phys. **92**, 015001 (2020).

[11] N. Brunner, D. Cavalcanti, S. Pironio, V. Scarani, and S. Wehner, Bell nonlocality, Rev. Mod. Phys. **86**, 419 (2014).

[12] A. Einstein, B. Podolsky, and N. Rosen, Can quantum-mechanical description of physical reality be considered complete? Phys. Rev. **47**, 777 (1935).

[13] A. Aspect, P. Grangier, and G. Roger, Experimental tests of realistic local theories via bell's theorem, Phys. Rev. Lett. **47**, 460 (1981).

[14] D. Bouwmeester, J.-W. Pan, M. Daniell, H. Weinfurter, and A. Zeilinger, Observation of three-photon greenberger-horne-zeilinger entanglement, Phys. Rev. Lett. **82**, 1345 (1999).

[15] D. Bouwmeester, J.-W. Pan, K. Mattle, M. Eibl, H. Weinfurter, and A. Zeilinger, Experimental quantum teleportation, Nature (London) **390**, 575 (1997).

[16] S. Slussarenko and G. J. Pryde, Photonic quantum information processing: A concise review, Appl. Phys. Rev. **6**, 041303 (2019).

[17] S. Lloyd and S. L. Braunstein, Quantum computation over continuous variables, Phys. Rev. Lett. **82**, 1784 (1999).

[18] L.-A. Wu, H. J. Kimble, J. L. Hall, and H. Wu, Generation of squeezed states by parametric down conversion, Phys. Rev. Lett. **57**, 2520 (1986).

[19] R. E. Slusher, L. W. Hollberg, B. Yurke, J. C. Mertz, and J. F. Valley, Observation of squeezed states generated by four-wave mixing in an optical cavity, Phys. Rev. Lett. **55**, 2409 (1985).

[20] H. Kimble, Squeezed states of light: An (incomplete) survey of experimental progress and prospects, Phys. Rep. **219**, 227 (1992).

[21] U. L. Andersen, T. Gehring, C. Marquardt, and G. Leuchs, 30 years of squeezed light generation, Phys. Scr. **91**, 053001 (2016).

[22] A. Furusawa, J. L. Sørensen, S. L. Braunstein, C. A. Fuchs, H. J. Kimble, and E. S. Polzik, Unconditional quantum teleportation, Science **282**, 706 (1998).

[23] R. Ukai, N. Iwata, Y. Shimokawa, S. C. Armstrong, A. Politi, J. Yoshikawa, P. van Loock, and A. Furusawa, Demonstration of unconditional one-way quantum computations for continuous variables, Phys. Rev. Lett. **106**, 240504 (2011).

[24] S. Yokoyama, R. Ukai, S. C. Armstrong, J. Yoshikawa, P. van Loock, and A. Furusawa, Demonstration of a fully tunable entangling gate for continuous-variable one-way quantum computation, Phys. Rev. A **92**, 032304 (2015).

[25] M. Yukawa, R. Ukai, P. van Loock, and A. Furusawa, Experimental generation of four-mode continuous-variable cluster states, Phys. Rev. A **78**, 012301 (2008).
[26] X. Su, S. Hao, X. Deng, L. Ma, M. Wang, X. Jia, C. Xie, and K. Peng, Gate sequence for continuous variable one-way quantum computation, Nat. Commun. **4**, 2828 (2013).
[27] Y. Wang, X. Su, H. Shen, A. Tan, C. Xie, and K. Peng, Toward demonstrating controlled-x operation based on continuous-variable four-partite cluster states and quantum teleporters, Phys. Rev. A **81**, 022311 (2010).
[28] X. Su, A. Tan, X. Jia, J. Zhang, C. Xie, and K. Peng, Experimental preparation of quadripartite cluster and greenberger-horne-zeilinger entangled states for continuous variables, Phys. Rev. Lett. **98**, 070502 (2007).
[29] Y. Miwa, R. Ukai, J. Yoshikawa, R. Filip, P. van Loock, and A. Furusawa, Demonstration of cluster-state shaping and quantum erasure for continuous variables, Phys. Rev. A **82**, 032305 (2010).
[30] X. Deng, Y. Xiang, C. Tian, G. Adesso, Q. He, Q. Gong, X. Su, C. Xie, and K. Peng, Demonstration of monogamy relations for Einstein-Podolsky-Rosen steering in Gaussian cluster states, Phys. Rev. Lett. **118**, 230501 (2017).
[31] X. Su, Y. Zhao, S. Hao, X. Jia, C. Xie, and K. Peng, Experimental preparation of eight-partite cluster state for photonic qumodes, Opt. Lett. **37**, 5178 (2012).
[32] S. Hao, X. Su, C. Tian, C. Xie, and K. Peng, Five-wave-packet quantum error correction based on continuous-variable cluster entanglement, Sci. Rep. **5**, 15462 (2015).
[33] H. Yonezawa, T. Aoki, and A. Furusawa, Demonstration of a quantum teleportation network for continuous variables, Nature (London) **431**, 430 (2004).
[34] T. Aoki, G. Takahashi, T. Kajiya, J. Yoshikawa, S. L. Braunstein, P. van Loock, and A. Furusawa, Quantum error correction beyond qubits, Nat. Phys. **5**, 541 (2009).
[35] J. Zhang, C. Xie, K. Peng, and P. van Loock, Anyon statistics with continuous variables, Phys. Rev. A **78**, 052121 (2008).
[36] N. C. Menicucci, Temporal-mode continuous-variable cluster states using linear optics, Phys. Rev. A **83**, 062314 (2011).
[37] R. N. Alexander, S. Yokoyama, A. Furusawa, and N. C. Menicucci, Universal quantum computation with temporal-mode bilayer square lattices, Phys. Rev. A **97**, 032302 (2018).
[38] R. N. Alexander, P. Wang, N. Sridhar, M. Chen, O. Pfister, and N. C. Menicucci, One-way quantum computing with arbitrarily large time-frequency continuous-variable cluster states from a single optical parametric oscillator, Phys. Rev. A **94**, 032327 (2016).
[39] N. C. Menicucci, X. Ma, and T. C. Ralph, Arbitrarily large continuous-variable cluster states from a single quantum nondemolition gate, Phys. Rev. Lett. **104**, 250503 (2010).
[40] B.-H. Wu, R. N. Alexander, S. Liu, and Z. Zhang, Quantum computing with multidimensional continuous-variable cluster states in a scalable photonic platform, Phys. Rev. Res. **2**, 023138 (2020).
[41] K. Fukui, W. Asavanant, and A. Furusawa, Temporal-mode continuous-variable three-dimensional cluster state for topologically protected measurement-based quantum computation, Phys. Rev. A **102**, 032614 (2020).
[42] R. Pooser and J. Jing, Continuous-variable cluster-state generation over the optical spatial mode comb, Phys. Rev. A **90**, 043841 (2014).
[43] N. C. Menicucci, S. T. Flammia, H. Zaidi, and O. Pfister, Ultracompact generation of continuous-variable cluster states, Phys. Rev. A **76**, 010302(R) (2007).
[44] H. Wang, K. Zhang, N. Treps, C. Fabre, J. Zhang, and J. Jing, Generation of hexapartite entanglement in a four-wave-mixing process with a spatially structured pump: Theoretical study, Phys. Rev. A **102**, 022417 (2020).
[45] R. Yang, J. Zhang, S. Zhai, K. Liu, J. Zhang, and J. Gao, Generating multiplexed entanglement frequency comb in a nondegenerate optical parametric amplifier, J. Opt. Soc. Am. B **30**, 314 (2013).
[46] R. Yang, J. Wang, J. Zhang, K. Liu, and J. Gao, Generation of continuous-variable spatial cluster entangled states in optical mode comb, J. Opt. Soc. Am. B **33**, 2424 (2016).
[47] J. Zhang, J. J. Wang, R. G. Yang, K. Liu, and J. R. Gao, Large-scale continuous-variable dual-rail cluster entangled state based on spatial mode comb, Opt. Express **25**, 27172 (2017).
[48] D. Barral, M. Walschaers, K. Bencheikh, V. Parigi, J. A. Levenson, N. Treps, and N. Belabas, Versatile photonic entanglement synthesizer in the spatial domain, Phys. Rev. Appl. **14**, 044025 (2020).
[49] M. V. Larsen, C. Chamberland, K. Noh, J. S. Neergaard-Nielsen, and U. L. Andersen, Fault-tolerant continuous-variable measurement-based quantum computation architecture, PRX Quantum **2**, 030325 (2021).
[50] C. Fabre and N. Treps, Modes and states in quantum optics, Rev. Mod. Phys. **92**, 035005 (2020).
[51] S. Yokoyama, R. Ukai, S. C. Armstrong, C. Sornphiphatphong, T. Kaji, S. Suzuki, J. Yoshikawa, H. Yonezawa, N. C. Menicucci, and A. Furusawa, Ultra-large-scale continuous-variable cluster states multiplexed in the time domain, Nat. Photonics **7**, 982 (2013).
[52] J. Yoshikawa, S. Yokoyama, T. Kaji, C. Sornphiphatphong, Y. Shiozawa, K. Makino, and A. Furusawa, Invited article: Generation of one-million-mode continuous-variable cluster state by unlimited time-domain multiplexing, APL Photonics **1**, 060801 (2016).
[53] W. Asavanant, Y. Shiozawa, S. Yokoyama, B. Charoensombutamon, H. Emura, R. N. Alexander, S. Takeda, J. Yoshikawa, N. C. Menicucci, H. Yonezawa, and A. Furusawa, Generation of time-domain-multiplexed two-dimensional cluster state, Science **366**, 373 (2019).
[54] M. V. Larsen, X. Guo, C. R. Breum, J. S. Neergaard-Nielsen, and U. L. Andersen, Deterministic generation of a two-dimensional cluster state, Science **366**, 369 (2019).
[55] W. Asavanant, B. Charoensombutamon, S. Yokoyama, T. Ebihara, T. Nakamura, R. N. Alexander, M. Endo, J. Yoshikawa, N. C. Menicucci, H. Yonezawa, and A. Furusawa, Time-domain-multiplexed measurement-based quantum operations with 25-MHz clock frequency, Phys. Rev. Appl. **16**, 034005 (2021).
[56] M. V. Larsen, X. Guo, C. R. Breum, J. S. Neergaard-Nielsen, and U. L. Andersen, Deterministic multi-mode gates on a scalable photonic quantum computing platform, Nat. Phys. **17**, 1018 (2021).
[57] M. Chen, N. C. Menicucci, and O. Pfister, Experimental realization of multipartite entanglement of 60 modes of a

quantum optical frequency comb, Phys. Rev. Lett. **112**, 120505 (2014).
[58] O. Pfister, Continuous-variable quantum computing in the quantum optical frequency comb, J. Phys. B: At., Mol. Opt. Phys. **53**, 012001 (2019).
[59] Y.-S. Ra, A. Dufour, M. Walschaers, C. Jacquard, T. Michel, C. Fabre, and N. Treps, Non-Gaussian quantum states of a multimode light field, Nat. Phys. **16**, 144 (2020).
[60] J. Roslund, R. M. de Araújo, S. Jiang, C. Fabre, and N. Treps, Wavelength-multiplexed quantum networks with ultrafast frequency combs, Nat. Photonics **8**, 109 (2014).
[61] Y. Cai, J. Roslund, G. Ferrini, F. Arzani, X. Xu, C. Fabre, and N. Treps, Multimode entanglement in reconfigurable graph states using optical frequency combs, Nat. Commun. **8**, 15645 (2017).
[62] O. Pinel, P. Jian, R. M. de Araújo, J. Feng, B. Chalopin, C. Fabre, and N. Treps, Generation and characterization of multimode quantum frequency combs, Phys. Rev. Lett. **108**, 083601 (2012).
[63] M. V. Larsen, X. Guo, C. R. Breum, J. S. Neergaard-Nielsen, and U. L. Andersen, Fiber-coupled epr-state generation using a single temporally multiplexed squeezed light source, npj Quantum Inf. **5**, 46 (2019).
[64] S. Gerke, J. Sperling, W. Vogel, Y. Cai, J. Roslund, N. Treps, and C. Fabre, Full multipartite entanglement of frequency-comb Gaussian states, Phys. Rev. Lett. **114**, 050501 (2015).
[65] T. Kouadou, F. Sansavini, M. Ansquer, J. Henaff, N. Treps, and V. Parigi, Spectrally shaped and pulse-by-pulse multiplexed multimode squeezed states of light, APL Photonics **8**, 086113 (2023).
[66] M. Pysher, Y. Miwa, R. Shahrokhshahi, R. Bloomer, and O. Pfister, Parallel generation of quadripartite cluster entanglement in the optical frequency comb, Phys. Rev. Lett. **107**, 030505 (2011).
[67] O. Kovalenko, Y.-S. Ra, Y. Cai, V. C. Usenko, C. Fabre, N. Treps, and R. Filip, Frequency-multiplexed entanglement for continuous-variable quantum key distribution, Photon. Res. **9**, 2351 (2021).
[68] C. Roh, G. Gwak, Y.-D. Yoon, and Y.-S. Ra, Generation of three-dimensional cluster entangled state, arXiv:2309.05437.
[69] S. Armstrong, J.-F. Morizur, J. Janousek, B. Hage, N. Treps, P. K. Lam, and H.-A. Bachor, Programmable multimode quantum networks, Nat. Commun. **3**, 1026 (2012).
[70] K. Liu, J. Guo, C. Cai, S. Guo, and J. Gao, Experimental generation of continuous-variable hyperentanglement in an optical parametric oscillator, Phys. Rev. Lett. **113**, 170501 (2014).
[71] C. Cai, L. Ma, J. Li, H. Guo, K. Liu, H. Sun, R. Yang, and J. Gao, Generation of a continuous-variable quadripartite cluster state multiplexed in the spatial domain, Photon. Res. **6**, 479 (2018).
[72] X. Wang and J. Jing, Deterministic entanglement of large-scale Hermite-Gaussian modes, Phys. Rev. Appl. **18**, 024057 (2022).
[73] H. Guo, N. Liu, Z. Li, R. Yang, H. Sun, K. Liu, and J. Gao, Generation of continuous-variable high-dimensional entanglement with three degrees of freedom and multiplexing quantum dense coding, Photon. Res. **10**, 2828 (2022).
[74] W. Wang, K. Zhang, and J. Jing, Large-scale quantum network over 66 orbital angular momentum optical modes, Phys. Rev. Lett. **125**, 140501 (2020).
[75] P. van Loock, C. Weedbrook, and M. Gu, Building Gaussian cluster states by linear optics, Phys. Rev. A **76**, 032321 (2007).
[76] T. Rudolph, Why I am optimistic about the silicon-photonic route to quantum computing, APL Photonics **2**, 030901 (2017).
[77] X. Ding, Y.-P. Guo, M.-C. Xu, R.-Z. Liu, G.-Y. Zou, J.-Y. Zhao, Z.-X. Ge, Q.-H. Zhang, H.-L. Liu, L.-J. Wang, M.-C. Chen, H. Wang, Y.-M. He, Y.-H. Huo, C.-Y. Lu, and J.-W. Pan, High-efficiency single-photon source above the loss-tolerant threshold for efficient linear optical quantum computing, arXiv:2311.08347.
[78] S. Bartolucci, P. Birchall, H. Bombín, H. Cable, C. Dawson, M. Gimeno-Segovia, E. Johnston, K. Kieling, N. Nickerson, M. Pant, F. Pastawski, T. Rudolph, and C. Sparrow, Fusion-based quantum computation, Nat. Commun. **14**, 912 (2023).
[79] U. Leonhardt, *Essential Quantum Optics: From Quantum Measurements to Black Holes* (Cambridge University Press, Cambridge, 2010).
[80] C. Weedbrook, S. Pirandola, R. García-Patrón, N. J. Cerf, T. C. Ralph, J. H. Shapiro, and S. Lloyd, Gaussian quantum information, Rev. Mod. Phys. **84**, 621 (2012).
[81] N. C. Menicucci, P. van Loock, M. Gu, C. Weedbrook, T. C. Ralph, and M. A. Nielsen, Universal quantum computation with continuous-variable cluster states, Phys. Rev. Lett. **97**, 110501 (2006).
[82] J. Yoshikawa, Y. Miwa, A. Huck, U. L. Andersen, P. van Loock, and A. Furusawa, Demonstration of a quantum nondemolition sum gate, Phys. Rev. Lett. **101**, 250501 (2008).
[83] Y. Shiozawa, J. Yoshikawa, S. Yokoyama, T. Kaji, K. Makino, T. Serikawa, R. Nakamura, S. Suzuki, S. Yamazaki, W. Asavanant, S. Takeda, P. van Loock, and A. Furusawa, Quantum nondemolition gate operations and measurements in real time on fluctuating signals, Phys. Rev. A **98**, 052311 (2018).
[84] S. L. Braunstein, Squeezing as an irreducible resource, Phys. Rev. A **71**, 055801 (2005).
[85] C. Bloch and A. Messiah, The canonical form of an antisymmetric tensor and its application to the theory of superconductivity, Nucl. Phys. **39**, 95 (1962).
[86] R. Simon, E. C. G. Sudarshan, and N. Mukunda, Gaussian pure states in quantum mechanics and the symplectic group, Phys. Rev. A **37**, 3028 (1988).
[87] R. Hudson, When is the wigner quasi-probability density non-negative? Rep. Math. Phys. **6**, 249 (1974).
[88] R. Filip, P. Marek, and U. L. Andersen, Measurement-induced continuous-variable quantum interactions, Phys. Rev. A **71**, 042308 (2005).
[89] Y. Miwa, J. Yoshikawa, N. Iwata, M. Endo, P. Marek, R. Filip, P. van Loock, and A. Furusawa, Exploring a new regime for processing optical qubits: Squeezing and unsqueezing single photons, Phys. Rev. Lett. **113**, 013601 (2014).
[90] N. C. Menicucci, S. T. Flammia, and P. van Loock, Graphical calculus for Gaussian pure states, Phys. Rev. A **83**, 042335 (2011).
[91] P. Horodecki, Separability criterion and inseparable mixed states with positive partial transposition, Phys. Lett. A **232**, 333 (1997).

[92] L.-M. Duan, G. Giedke, J. I. Cirac, and P. Zoller, Inseparability criterion for continuous variable systems, Phys. Rev. Lett. **84**, 2722 (2000).

[93] R. Simon, Peres-Horodecki separability criterion for continuous variable systems, Phys. Rev. Lett. **84**, 2726 (2000).

[94] P. van Loock and A. Furusawa, Detecting genuine multipartite continuous-variable entanglement, Phys. Rev. A **67**, 052315 (2003).

[95] R. Raussendorf and H. J. Briegel, A one-way quantum computer, Phys. Rev. Lett. **86**, 5188 (2001).

[96] S. Takeda, K. Takase, and A. Furusawa, On-demand photonic entanglement synthesizer, Sci. Adv. **5**, eaaw4530 (2019).

[97] W. Asavanant and A. Furusawa, *Optical Quantum Computers: A Route to Practical Continuous Variable Quantum Information Processing* (AIP Publishing, Melville, NY, 2022).

[98] A. Furusawa and P. van Loock, *Quantum Teleportation and Entanglement: A Hybrid Approach to Optical Quantum Information Processing* (Wiley, Hoboken, NJ, 2011).

[99] F. Mondain, T. Lunghi, A. Zavatta, E. Gouzien, F. Doutre, M. D. Micheli, S. Tanzilli, and V. D'Auria, Chip-based squeezing at a telecom wavelength, Photon. Res. **7**, A36 (2019).

[100] Y. Piétri, L. Trigo Vidarte, M. Schiavon, L. Vivien, P. Grangier, A. Rhouni, and E. Diamanti, Experimental demonstration of Continuous-Variable Quantum Key Distribution with a silicon photonics integrated receiver, arXiv:2311.03978.

[101] M. J. Collett and C. W. Gardiner, Squeezing of intracavity and traveling-wave light fields produced in parametric amplification, Phys. Rev. A **30**, 1386 (1984).

[102] J. Yoshikawa, W. Asavanant, and A. Furusawa, Purification of photon subtraction from continuous squeezed light by filtering, Phys. Rev. A **96**, 052304 (2017).

[103] P. Du, Y. Wang, K. Liu, R. Yang, and J. Zhang, Generation of large-scale continuous-variable cluster states multiplexed both in time and frequency domains, Opt. Express **31**, 7535 (2023).

[104] P. Du, J. Zhang, T. Zhang, R. Yang, and J. Gao, A complete continuous-variable quantum computation architecture: from cluster state generation to fault-tolerant accomplishment, arXiv:2312.13877.

[105] R. Yang, J. Zhang, I. Klich, C. González-Arciniegas, and O. Pfister, Spatiotemporal graph states from a single optical parametric oscillator, Phys. Rev. A **101**, 043832 (2020).

[106] Y. Zhou, J. Zhao, Z. Shi, S. M. H. Rafsanjani, M. Mirhosseini, Z. Zhu, A. E. Willner, and R. W. Boyd, Hermite–Gaussian mode sorter, Opt. Lett. **43**, 5263 (2018).

[107] G. Labroille, B. Denolle, P. Jian, P. Genevaux, N. Treps, and J.-F. Morizur, Efficient and mode selective spatial mode multiplexer based on multi-plane light conversion, Opt. Express **22**, 15599 (2014).

[108] P. Boucher, C. Fabre, G. Labroille, and N. Treps, Spatial optical mode demultiplexing as a practical tool for optimal transverse distance estimation, Optica **7**, 1621 (2020).

[109] H. Vahlbruch, M. Mehmet, K. Danzmann, and R. Schnabel, Detection of 15 dB squeezed states of light and their application for the absolute calibration of photoelectric quantum efficiency, Phys. Rev. Lett. **117**, 110801 (2016).

[110] M. Mehmet, S. Ast, T. Eberle, S. Steinlechner, H. Vahlbruch, and R. Schnabel, Squeezed light at 1550 nm with a quantum noise reduction of 12.3 dB, Opt. Express **19**, 25763 (2011).

[111] B. Shajilal, O. Thearle, A. Tranter, Y. Lu, E. Huntington, S. Assad, P. K. Lam, and J. Janousek, 12.6 dB squeezed light at 1550 nm from a bow-tie cavity for long-term high duty cycle operation, Opt. Express **30**, 37213 (2022).

[112] C. Kim and P. Kumar, Quadrature-squeezed light detection using a self-generated matched local oscillator, Phys. Rev. Lett. **73**, 1605 (1994).

[113] J. Amari, J. Takai, and T. Hirano, Highly efficient measurement of optical quadrature squeezing using a spatial light modulator controlled by machine learning, Opt. Continuum **2**, 933 (2023).

[114] T. Serikawa, J. Yoshikawa, K. Makino, and A. Frusawa, Creation and measurement of broadband squeezed vacuum from a ring optical parametric oscillator, Opt. Express **24**, 28383 (2016).

[115] S. Ast, M. Mehmet, and R. Schnabel, High-bandwidth squeezed light at 1550 nm from a compact monolithic PPKTP cavity, Opt. Express **21**, 13572 (2013).

[116] T. Kashiwazaki, T. Yamashima, N. Takanashi, A. Inoue, T. Umeki, and A. Furusawa, Fabrication of low-loss quasi-single-mode PPLN waveguide and its application to a modularized broadband high-level squeezer, Appl. Phys. Lett. **119**, 251104 (2021).

[117] A. Inoue, T. Kashiwazaki, T. Yamashima, N. Takanashi, T. Kazama, K. Enbutsu, K. Watanabe, T. Umeki, M. Endo, and A. Furusawa, Toward a multi-core ultra-fast optical quantum processor: 43-GHz bandwidth real-time amplitude measurement of 5-dB squeezed light using modularized optical parametric amplifier with 5G technology, Appl. Phys. Lett. **122**, 104001 (2023).

[118] T. Kashiwazaki, T. Yamashima, K. Enbutsu, T. Kazama, A. Inoue, K. Fukui, M. Endo, T. Umeki, and A. Furusawa, Over-8-dB squeezed light generation by a broadband waveguide optical parametric amplifier toward fault-tolerant ultrafast quantum computers, Appl. Phys. Lett. **122**, 234003 (2023).

[119] J. F. Tasker, J. Frazer, G. Ferranti, E. J. Allen, L. F. Brunel, S. Tanzilli, V. D'Auria, and J. C. F. Matthews, Silicon photonics interfaced with integrated electronics for 9 GHz measurement of squeezed light, Nat. Photonics **15**, 11 (2021).

[120] V. D. Vaidya, B. Morrison, L. G. Helt, R. Shahrokshahi, D. H. Mahler, M. J. Collins, K. Tan, J. Lavoie, A. Repingon, M. Menotti, N. Quesada, R. C. Pooser, A. E. Lita, T. Gerrits, S. W. Nam, and Z. Vernon, Broadband quadrature-squeezed vacuum and nonclassical photon number correlations from a nanophotonic device, Sci. Adv. **6**, eaba9186 (2020).

[121] B. W. Walshe, R. N. Alexander, N. C. Menicucci, and B. Q. Baragiola, Streamlined quantum computing with macronode cluster states, Phys. Rev. A **104**, 062427 (2021).

[122] B. W. Walshe, L. J. Mensen, B. Q. Baragiola, and N. C. Menicucci, Robust fault tolerance for continuous-variable cluster states with excess antisqueezing, Phys. Rev. A **100**, 010301(R) (2019).

[123] H. Lee, T. Chen, J. Li, O. Painter, and K. J. Vahala, Ultra-low-loss optical delay line on a silicon chip, Nat. Commun. **3**, 867 (2012).

[124] A. Yariv and P. Yeh, *Photonics: Optical Electronics in Modern Communications (The Oxford Series in Electrical and Computer Engineering)* (Oxford University Press, New York, 2006).

[125] G. Son, S. Han, J. Park, K. Kwon, and K. Yu, High-efficiency broadband light coupling between optical fibers and photonic integrated circuits, Nanophotonics **7**, 1845 (2018).
[126] T. Serikawa and A. Furusawa, Excess loss in homodyne detection originating from distributed photocarrier generation in photodiodes, Phys. Rev. Appl. **10**, 064016 (2018).
[127] Y. Shaked, Y. Michael, R. Z. Vered, L. Bello, M. Rosenbluh, and A. Pe'er, Lifting the bandwidth limit of optical homodyne measurement with broadband parametric amplification, Nat. Commun. **9**, 609 (2018).
[128] R. Nehra, R. Sekine, L. Ledezma, Q. Guo, R. M. Gray, A. Roy, and A. Marandi, Few-cycle vacuum squeezing in nanophotonics, Science **377**, 1333 (2022).
[129] C. H. Bennett, G. Brassard, C. Crépeau, R. Jozsa, A. Peres, and W. K. Wootters, Teleporting an unknown quantum state via dual classical and Einstein-Podolsky-Rosen channels, Phys. Rev. Lett. **70**, 1895 (1993).
[130] L. Vaidman, Teleportation of quantum states, Phys. Rev. A **49**, 1473 (1994).
[131] S. L. Braunstein and H. J. Kimble, Teleportation of continuous quantum variables, Phys. Rev. Lett. **80**, 869 (1998).
[132] D. Gottesman, A. Kitaev, and J. Preskill, Encoding a qubit in an oscillator, Phys. Rev. A **64**, 012310 (2001).
[133] N. C. Menicucci, Fault-tolerant measurement-based quantum computing with continuous-variable cluster states, Phys. Rev. Lett. **112**, 120504 (2014).
[134] K. Fukui, A. Tomita, and A. Okamoto, Analog quantum error correction with encoding a qubit into an oscillator, Phys. Rev. Lett. **119**, 180507 (2017).
[135] J. E. Bourassa, R. N. Alexander, M. Vasmer, A. Patil, I. Tzitrin, T. Matsuura, D. Su, B. Q. Baragiola, S. Guha, G. Dauphinais *et al.*, Blueprint for a scalable photonic fault-tolerant quantum computer, Quantum **5**, 392 (2021).
[136] I. Tzitrin, T. Matsuura, R. N. Alexander, G. Dauphinais, J. E. Bourassa, K. K. Sabapathy, N. C. Menicucci, and I. Dhand, Fault-tolerant quantum computation with static linear optics, PRX Quantum **2**, 040353 (2021).
[137] K. Fukui, A. Tomita, A. Okamoto, and K. Fujii, High-threshold fault-tolerant quantum computation with analog quantum error correction, Phys. Rev. X **8**, 021054 (2018).
[138] H. J. Kimble, The quantum internet, Nature (London) **453**, 1023 (2008).
[139] C. Portmann and R. Renner, Security in quantum cryptography, Rev. Mod. Phys. **94**, 025008 (2022).
[140] P. van Loock and S. L. Braunstein, Multipartite entanglement for continuous variables: A quantum teleportation network, Phys. Rev. Lett. **84**, 3482 (2000).
[141] M. Hillery, V. Bužek, and A. Berthiaume, Quantum secret sharing, Phys. Rev. A **59**, 1829 (1999).
[142] D. Gottesman, Theory of quantum secret sharing, Phys. Rev. A **61**, 042311 (2000).
[143] H.-K. Lau and C. Weedbrook, Quantum secret sharing with continuous-variable cluster states, Phys. Rev. A **88**, 042313 (2013).
[144] N. Walk and J. Eisert, Sharing classical secrets with continuous-variable entanglement: Composable security and network coding advantage, PRX Quantum **2**, 040339 (2021).
[145] N. C. Menicucci, B. Q. Baragiola, T. F. Demarie, and G. K. Brennen, Anonymous broadcasting of classical information with a continuous-variable topological quantum code, Phys. Rev. A **97**, 032345 (2018).
[146] B. Q. Baragiola, G. Pantaleoni, R. N. Alexander, A. Karanjai, and N. C. Menicucci, All-Gaussian universality and fault tolerance with the Gottesman-Kitaev-Preskill code, Phys. Rev. Lett. **123**, 200502 (2019).
[147] N. Killoran, T. R. Bromley, J. M. Arrazola, M. Schuld, N. Quesada, and S. Lloyd, Continuous-variable quantum neural networks, Phys. Rev. Res. **1**, 033063 (2019).
[148] G. Verdon, J. M. Arrazola, K. Brádler, and N. Killoran, A Quantum Approximate Optimization Algorithm for continuous problems, arXiv:1902.00409.
[149] M. Dakna, T. Anhut, T. Opatrný, L. Knöll, and D.-G. Welsch, Generating Schrödinger-cat-like states by means of conditional measurements on a beam splitter, Phys. Rev. A **55**, 3184 (1997).
[150] T. Serikawa, J. Yoshikawa, S. Takeda, H. Yonezawa, T. C. Ralph, E. H. Huntington, and A. Furusawa, Generation of a cat state in an optical sideband, Phys. Rev. Lett. **121**, 143602 (2018).
[151] M. Walschaers, S. Sarkar, V. Parigi, and N. Treps, Tailoring non-Gaussian continuous-variable graph states, Phys. Rev. Lett. **121**, 220501 (2018).
[152] M. Walschaers, Non-Gaussian quantum states and where to find them, PRX Quantum **2**, 030204 (2021).
[153] M. Walschaers, C. Fabre, V. Parigi, and N. Treps, Entanglement and Wigner function negativity of multimode non-Gaussian states, Phys. Rev. Lett. **119**, 183601 (2017).
[154] M. Walschaers, V. Parigi, and N. Treps, Practical framework for conditional non-Gaussian quantum state preparation, PRX Quantum **1**, 020305 (2020).
[155] M. Walschaers, C. Fabre, V. Parigi, and N. Treps, Statistical signatures of multimode single-photon-added and -subtracted states of light, Phys. Rev. A **96**, 053835 (2017).
[156] M. Walschaers and N. Treps, Remote generation of Wigner negativity through Einstein-Podolsky-Rosen steering, Phys. Rev. Lett. **124**, 150501 (2020).
[157] T. Sonoyama, K. Takahashi, B. Charoensombutamon, S. Takasu, K. Hattori, D. Fukuda, K. Fukui, K. Takase, W. Asavanant, J. Yoshikawa, M. Endo, and A. Furusawa, Non-Gaussian-state generation with time-gated photon detection, Phys. Rev. Res. **5**, 033156 (2023).
[158] W. Asavanant, K. Fukui, A. Sakaguchi, and A. Furusawa, Switching-free time-domain optical quantum computation with quantum teleportation, Phys. Rev. A **107**, 032412 (2023).
[159] M. V. Larsen, J. S. Neergaard-Nielsen, and U. L. Andersen, Architecture and noise analysis of continuous-variable quantum gates using two-dimensional cluster states, Phys. Rev. A **102**, 042608 (2020).
[160] A. Sakaguchi, S. Konno, F. Hanamura, W. Asavanant, K. Takase, H. Ogawa, P. Marek, R. Filip, J. Yoshikawa, E. Huntington, H. Yonezawa, and A. Furusawa, Nonlinear feedforward enabling quantum computation, Nat. Commun. **14**, 3817 (2023).
[161] C. S. Hamilton, R. Kruse, L. Sansoni, S. Barkhofen, C. Silberhorn, and I. Jex, Gaussian boson sampling, Phys. Rev. Lett. **119**, 170501 (2017).
[162] I. Tzitrin, J. E. Bourassa, N. C. Menicucci, and K. K. Sabapathy, Progress towards practical qubit computation us-

ing approximate gottesman-kitaev-preskill codes, Phys. Rev. A **101**, 032315 (2020).

[163] K. Takase, K. Fukui, A. Kawasaki, W. Asavanant, M. Endo, J. Yoshikawa, P. van Loock, and A. Furusawa, Gottesman-Kitaev-Preskill qubit synthesizer for propagating light, npj Quantum Inf. **9**, 98 (2023).

[164] A. I. Lvovsky, P. Grangier, A. Ourjoumtsev, V. Parigi, M. Sasaki, and R. Tualle-Brouri, Production and applications of non-Gaussian quantum states of light, arXiv:2006.16985.

[165] C. E. Lopetegui, M. Gessner, M. Fadel, N. Treps, and M. Walschaers, Homodyne detection of non-Gaussian quantum steering, PRX Quantum **3**, 030347 (2022).